Summary:
Experiments in Confinement and Wave-Plasma Interaction

F.C.Schüller

FOM-Instituut voor Plasmafysica, Association Euratom-FOM
Partner in the Trilateral Euregio Cluster
P.O.Box 1207, 3430BE Nieuwegein, The Netherlands

Abstract: The paper summarizes the results presented at the IAEA Fusion Energy Conference 2002 with respect to the performance and confinement of tokamaks, spherical tokamaks, stellarators, reversed field pinches and mirrors. Transport, internal transport barriers, methods to control pressure- and current density-profiles by auxiliary heating and non-inductive current drive will be discussed and compared to the predictions for ITER. On base of the results presented at this conference it can be concluded that one has confidence that the ITER performance specifications will be achieved in the future. Marked progress on alternative confinement concepts can be noted as well.

1. Performance in Tokamak Confinement

The most pressing question in experimental tokamak physics during the last years has been: can we be sure that ITER will reach simultaneously a number of parameters. Parameters that are necessary for the proof that the ITER-project will deliver and confirm that nuclear fusion based on the tokamak concept is a viable route to a new and highly needed energy supply.
A successful steady state plasma in ITER requires: 100% non-inductive current drive (f_{CD}= 1.0), from which 55% is bootstrap current (f_{BS}=0.55) at a normalized $ß_N$ of 3.2 and an H-factor of 1.5 with a line averaged density that is 80% of the Greenwald density (N_{GW}=0.8) and with radiative losses above 80% of the total heat-loss. (γ=0.8). After the previous IAEA conference in Sorrento one could already answer this question in a reasonably positive way [1]. Since then the confidence has grown even further based on experiments on JT-60U, JET, TS, DIII-D and ASDEX-U.
Very impressive results were obtained in JT-60U [2] where one reached a world record in the reactor criterion $nT\tau_E$ of $3.1x10^{20}$ $keVm^{-3}$ s in a discharge with full non-inductive current drive. See FIG. 1.

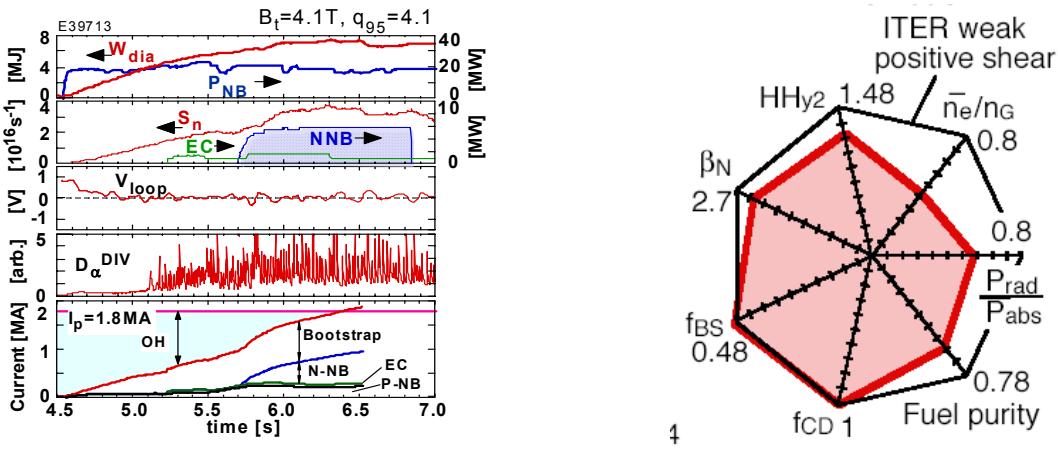

FIG. 1: JT-60U world record in $nT\tau_E$ ($3.1x10^{20}$ $keVm^{-3}$ s) and the position on the ITER-parameter diagram of that same pulse [2].

Comparison with a standard scenario ITER-plasma was also made in JT-60U. High triangularity (δ) at relatively low current and magnetic field made it possible to maintain $ß_N$ =2.7 during 70 confinement times (FIG. 2). High triangularity as foreseen for ITER turns out to be beneficial for the performance of all tokamaks now that the experiments are directed towards ITER–shape. A good example of that is shown in FIG. 3 of a record pulse in JET [3].

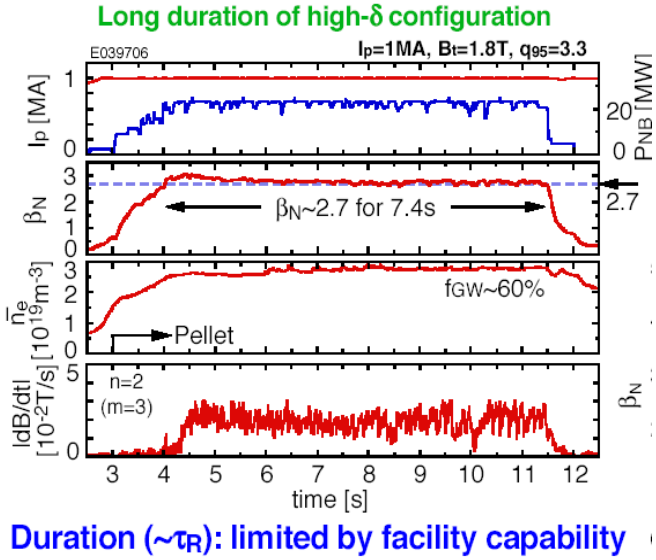

FIG. 2. High $ß_N$ =2.7 could be maintained for 70 times τ_E in high triangularity plasmas in JT-60U [2].

SHAPING	JET "ITER shape" Pulse No: 53299, 2.5MA/2.7T	ITER
$H_{98\,(y,2)}$	0.91	1.0
$\beta_{N,th}$	1.90	1.81
n_e / n_{GW}	1.1	0.85
Z_{eff}	1.5	1.7
P_{rad} / P_{tot}	0.40	0.58
κ, δ	1.74, 0.48	1.84, 0.5
q_{95}	3.2	3.0
τ_{pulse} / τ_E	15	110

JG01.416-1c

FIG. 3.a. High triangularity brought JET[3] to the achievement of parameters equal to or even exceeding those projected for ITER.

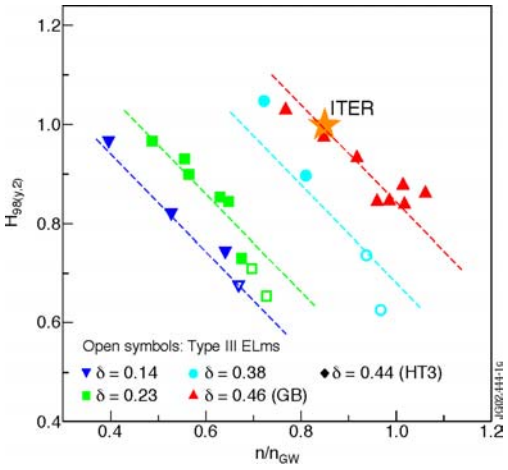

FIG. 3.b. The $H_{98,y2}$-factor of JET [3] as function of N_{GW} for various values of triangularity. The maximum density at which $H_{98,y2}$ can be kept at 1 is more than doubled between δ=0.14 and 0.46

In DIII-D [4] impressive results were obtained in "Advanced Tokamak scenarios (AT)" with slightly negative shear *). The record value of $ß_N$ H_{98} exceeding 10 for 4 times τ_E has been made possible by removing stray magnetic fields. A high value of plasma rotation could therefore be maintained, which suppressed MHD-modes and raised ß to values equal to the ideal wall-limit. See FIG. 4. At somewhat lower values of $ß_N$ H_{98} > 7 these AT-plasmas could be even maintained during 2 seconds, i.e. tens of τ_E at f_{CD} =0.9. These achievements show that AT-scenarios are as promising as standard ITER scenarios. The next step needed for real stationary high $ß_N$ H_{98} AT-plasmas is the suppression of NTM-like modes. Also on this issue the DIII-D team has made important progress as will be shown in par.5.
High triangularity brought also ASDEX-U [5] to record values of $ß_N$ H_{98} around 10 (FIG. 5).

**) ACRONYMS are listed at the end.*

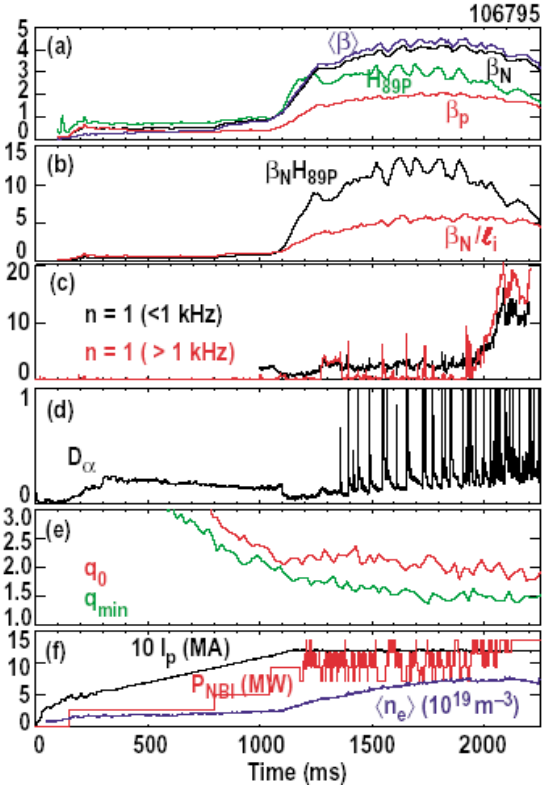

FIG. 4. A record value of $\beta_N H_{98}$ >10 has been obtained in an AT-scenario pulse of DIII-D during 4 confinement times [4]. The high β_N of 4 is close to the ideal wall-limit and made possible by strayfield compensation. The non-inductive current fraction is 0.85. NTM-like modes destroy the good confinement at t= 1.9 s.

2. Transport in Tokamaks (General)

On this conference it became clear that a large majority of fusion physicists are convinced that drift-wave turbulence is the mechanism responsible for turbulent transport in tokamaks. Many experimental features can be explained by drift-wave turbulence:

- Simulated profiles agree often very well with experimental temperature profiles;
- The observation of profile stiffness can well be explained;
- Good agreement with some measured heat-pulse propagation has been found;
- Good confinement, observed when density profiles become peaked, blends well with ITG predictions as function of l_n / l_T;
- Recently: good agreement between theoretical and experimental correlation length and times has been found and reported on this conference [6].

Nevertheless there are experimental and theoretical arguments that not everything is said with drift-wave theory. Especially during theory sessions of this conference this lead to hot debate:

- Drift-wave simulations even with sometimes arbitrary adaptations cannot in all cases explain profiles;
- The strong experimental fact of inward particle convection does not square easily with most drift-wave theories;
- The very clear existence of ITBs close to or at rational q-values only follows naturally from drift-wave theory if one accepts the theory of zonal flows and/or E x B-shear. The difficulty with this is what is cause or consequence?

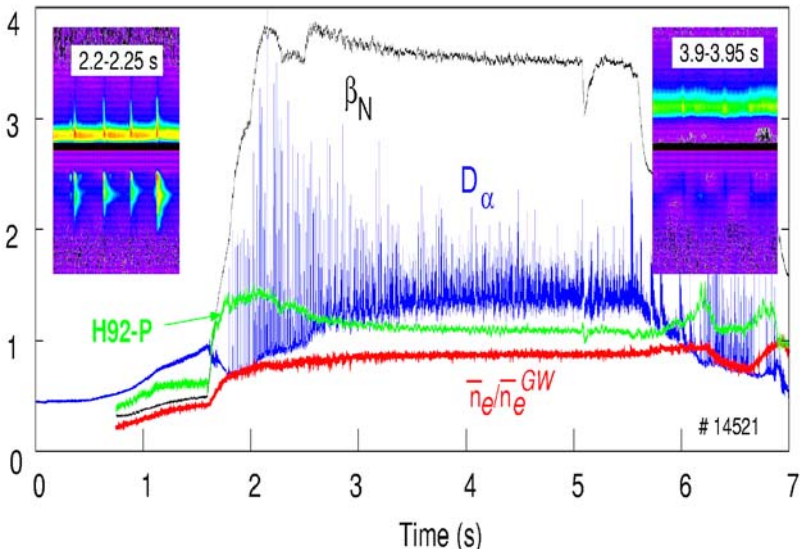

FIG. 5. β_N H_{98} close to 10 in ASDEX-U [5] has been achieved by high triangularity $\delta \approx 0.42$ and combined with benign Type II ELM's and N_{GW} =0.85 and maintained during 40 confinement times.

Experimentally a strong link between heat diffusivity and momentum diffusivity has always been observed. A local barrier for heat transport can therefore be expected to be accompanied by a barrier for toroidal momentum causing E x B-shear.

- Last but not least there is the question of fluctuating magnetic fields. These are only partially taken into account in electromagnetic extensions of the originally purely electrostatic turbulence models. For instance the temperature fluctuations predicted by drift-wave theory mean also fluctuations in resistivity and thereby fluctuations in current density. If these induce magnetic field fluctuations of only 10^{-4} of the main magnetic field, as observed experimentally, large areas of magnetic stochasticity will arise. The time dependant field line tracing, which is required to assess the effect, has not yet been included.

As this is a summary of experimental results and not of theory, only two examples of relevant experimental evidence will be given. The issue of ITBs will be treated in the next paragraph.

2.1 Profile Stiffness and Heat Pulse Propagation

The phenomenon of profile stiffness is observed in many tokamaks. An example is shown in FIG. 6. In fact it was already noted in the mid eighties in JET and lead then to the development of the Rebut-Lallia-Watkins (RLW) model. Any change in heat-deposition and power will lead to an overall change in temperature but not in the temperature gradient length, L_T. This couples the central temperature strongly to the edge temperature.

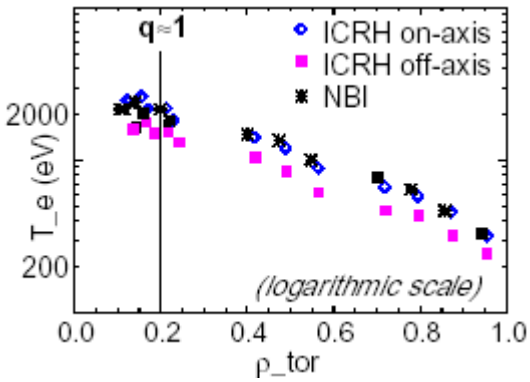

FIG. 6. Profile stiffness in ASDEX-U [5]: independent of heat deposition radius or heating method one finds the same value of the temperature gradient length L_T. For many machines the ratio L_T/R is around 10.

The ASDEX-team [7] explains the observation of profile stiffness by defining an electron heat-diffusivity, similar to the RLW-model, as:

$$\chi_e = \chi_{e0} + q\lambda T_e^{3/2}\left(\frac{1}{L_{T_e}} - \left(\frac{1}{L_{T_e}}\right)_{crit}\right) H\left(\frac{1}{L_{T_e}} - \left(\frac{1}{L_{T_e}}\right)_{crit}\right)$$

This model can be studied experimentally by comparing the electron heat diffusivity from local power balance with the one derived from heat-wave propagation measurements:

$$\chi_e^{PB} = -\frac{q_e}{n_e \nabla T_e}; \qquad \chi_e^{HP} = \chi_e^{PB} + \frac{\partial \chi_e}{\partial \nabla T_e}\nabla T$$

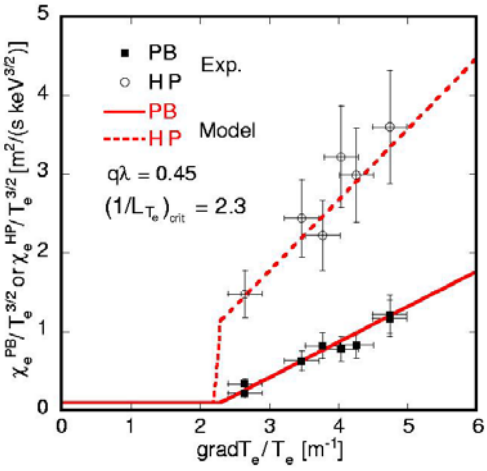

FIG 7. Comparison between electron heat-diffusivities from local power balance and heat-wave propagation in ASDEX-U [7].

This comparison indicates that the values found for L_{Te} are in good agreement with the predictions for the TEM-mode more than those for the ETG-mode.

2.2 Correlation Lengths and Times and Zonal Flows in DIII-D

A more direct confirmation of the validity of drift-wave predictions is the comparison between the measured values of correlation lengths/times and theoretically predicted values as done in DIII-D [6]. The measurements were made by correlation reflectometry (radial) and BES (poloidal). One finds quantitative agreement with the correlation lengths predicted by the giro-fluid code GRYFFIN and the giro-kinetic code GYRO. The correlation lengths roughly scales with 5-10 ρ_S. However in absolute value the fluctuation amplitude and the resulting flux differ with a factor 2-4 from experimental values. The electrostatic giro-kinetic PIC-code UCAN-3D allows the inclusion of self-generated, zonal, flows. Without these flows UCAN predicts correlation lengths that are one order of magnitude larger than the experimental ones, but with inclusion of zonal flows one gets good agreement. See FIG. 8. These zonal flows are measured by poloidal and radial phase shifts of low m-modes in the plasma edge. During a L-to-H transition one observes an inversion of the mode rotation over a distance of only a few cm inside the separatrix.

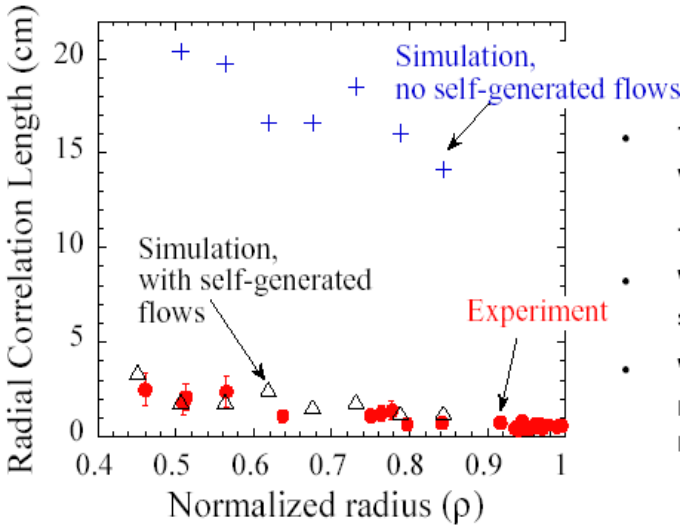

FIG. 8. Comparison [6] between radial correlation lengths measured in DIII-D (red) with the predictions of the 3D giro-kinetic PIC-code UCAN with (black) and without (blue) the inclusion of self-generated, zonal, flows

3. Internal Transport Barriers (ITB)

The study of ITBs was very much a focus point of the conference. The experimental observations can differ quite markedly between different devices, which lead to confusion and debate.

1. Various forms: ITBs can be observed in the profiles of electron- and ion-temperatures, of density and of plasma rotation in the form of localized jumps, i.e. local areas with very small gradient lengths. Heat-pulse propagation indicates a very much slower propagation across an ITB [8], [9]. See FIG. 9. The ITBs for various quantities can occur at the same place and time but not necessarily. For instance in the spherical tokamak MAST [10] they occur all simultaneously. See FIG. 10.

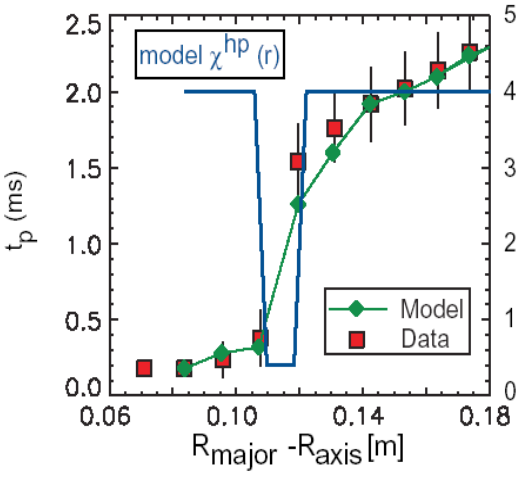

FIG.9. The delay in heat-pulse arrival time t_p across a thermal barrier in Alcator C-mod [8]

In general there is the opinion that at least e-ITBs are different from i-ITBs. ITBs are not restricted to standard tokamaks. With more or less the same characteristics they have been observed in stellarators and spherical tokamaks.

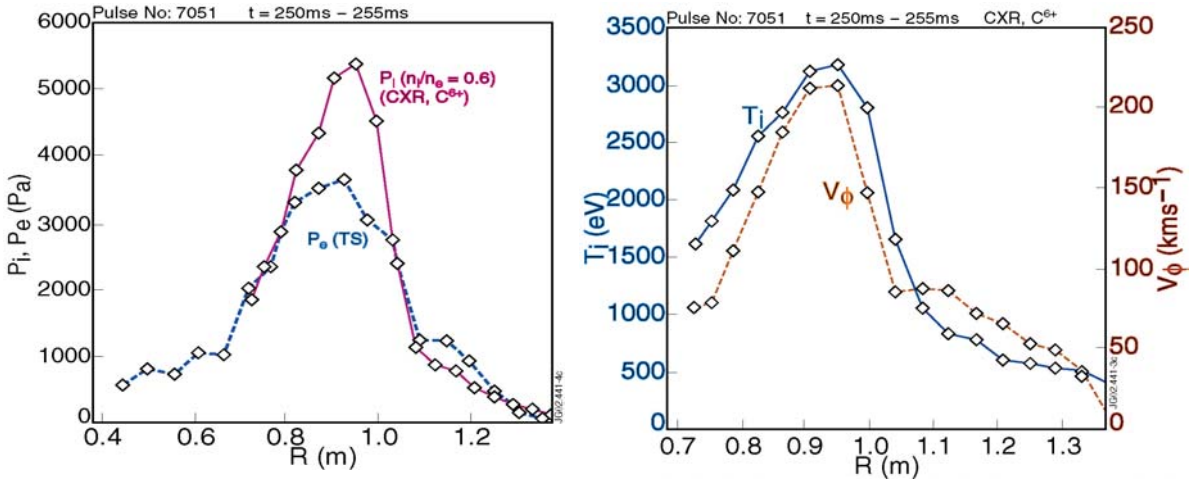

FIG. 10. The simultaneous barrier for electron-and ion-energy transport and toroidal momentum-transport in the spherical tokamak MAST [10].

2. <u>The relation to rational q-values.</u> Although not accepted by all teams it is generally believed that at least e(lectron)-ITBs exist at or close to rational q-values. This has been observed for the first time in RTP and JT-60 in the mid nineties and since then confirmed in JET, TEXTOR, T-10 and the stellarators W7-AS and TJ-II. The Dutch team at

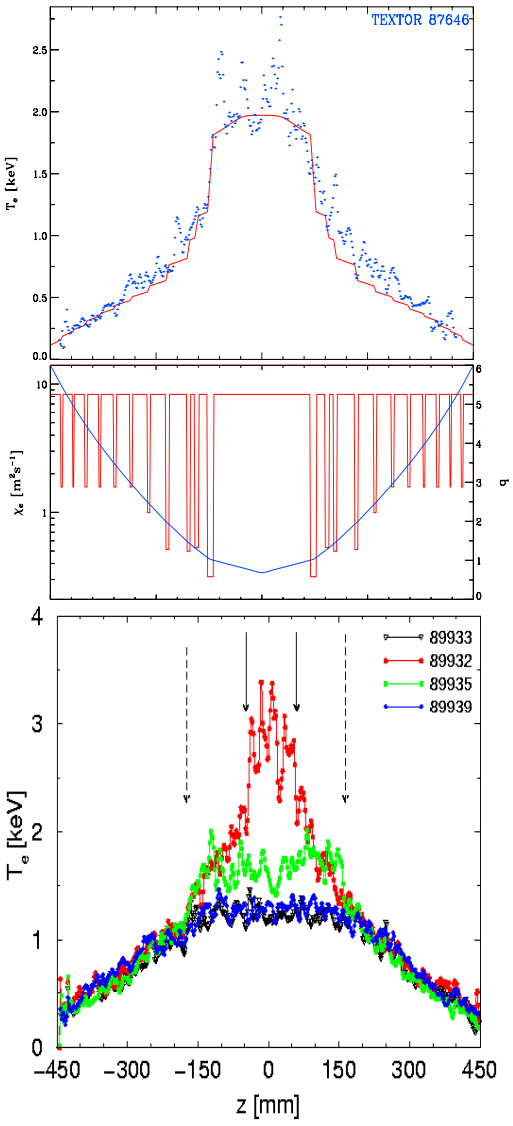

FIG. 11.a. The comparison between the RTP-model (in red χ eff = χ (q)) and the Thomson scattering T_e profile (blue) in TEXTOR [11] during a L-mode ECR-heated plasma. The q=1 barrier is clearly visible on the predicted location as well as the absolute height of the profile.

FIG. 11.b. Two simultaneous barriers in TEXTOR during a very low central shear pulse with ECRH. The various colors indicate profiles with different EC-deposition radius in respect to the barrier locations (arrows)

TEXTOR (previously at RTP) proposes [11] that for electrons there exist in principle e-ITBs at all low m/n-values of q but depending on shear, heat-flux and diagnostic resolution these are not always visible. Multiple e-ITBs are observed in TEXTOR (see FIG. 11) and in W7-AS [12].
In a NCS-pulse of JET [13] two e-ITBs occur at the two radii where q=2 at both sides of q_{min}. See FIG. 12. The relation between q (ρ) and i(on)-ITBs is much less clear.

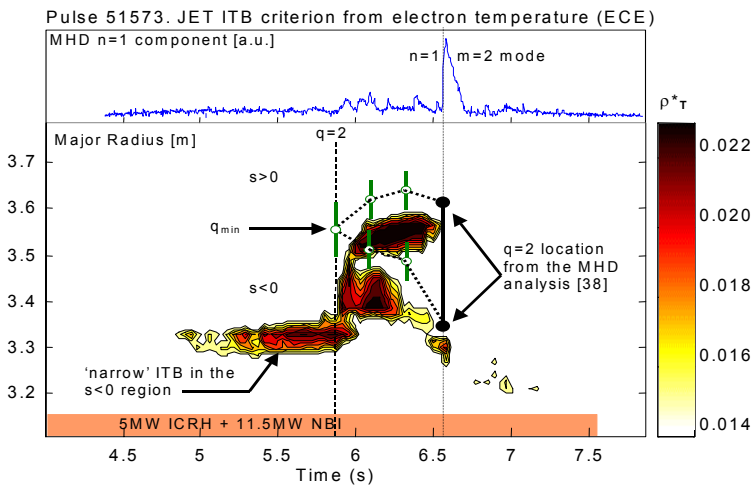

FIG. 12. The location of the e-ITB in a NCS-pulse in JET [13] with colour-coding giving the value of ρ. The double barrier is located at the 2 radii where q=2 at both sides of q_{min} .*

3. <u>The relation with (negative) shear.</u> Low or negative shear (NCS) seems to be beneficial for i-ITBs. They arise often at the radius of q_{min} in case of NCS plasmas but extend than inwards where the shear is negative. Their width is in general broader than of e-ITBs. In the strongly negative shear plasmas with "current holes" vigorous i- and e-ITBs are observed. However both the position and the width of the i-ITBs are not very different for the quite different q-profiles before the current hole develops (low NCS) and during the hole (strong NCS) [14]. See FIG. 13. Following the RTP-model that the width of e-ITBs is only dependant on δq, it is logical and observed that low shear gives large widths. The behaviour of I-ITBs is clearly different.

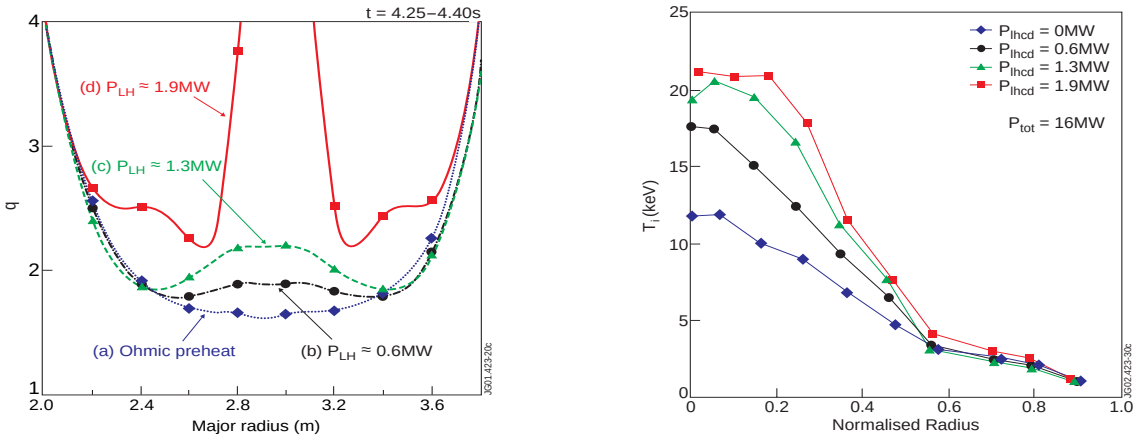

FIG. 13. The evolution of an i-ITB in JET during the birth of a 'current hole' in JET [14] caused by increasing levels of LHCD. The location of the foot-point of the ITB does not change whilst the q-profile (from MSE-measurements) changes considerably.

4. <u>The relation with velocity shear and zonal flows.</u> In many cases it has been observed that an area of strong velocity shear coincides with mainly i-ITB. The elegant explanation is that such velocity shear shreds turbulent eddies and is therefore the cause of the i-ITB. As said before: if there exists a link between momentum-ITB and energy-ITB the coincidence between velocity shear and i-ITB may have a common cause instead of one being the cause of the other. Measurements with high temporal and spatial resolution are necessary to resolve this question. Theory on the momentum-balance and anomalous viscosity is anyhow underdeveloped.

5. <u>Power threshold.</u> Many teams claim that there exists a power threshold for ITBs. The case for that seems to be stronger for ions than for electrons. The RTP-model for e-ITBs does not require a threshold. The JET-team originally thought otherwise but now regards their

database to be less clear for electrons. One of the difficulties is that collisional electron-ion energy exchange at both sides of the barrier modifies the fluxes across the barrier.
6. The ρ* -criterion. The JET-team [15] has introduced the criterion that one can speak of an ITB when $\rho^* = \rho_s / L_T > 0.014$. Theory of drift-wave turbulence gives some justification for this. However this definition has also an empirical character and can be in practice influenced by the spatial resolution of the diagnostic from which one derives the value of L_T.

4. Heating and Current Drive by Electro Magnetic Waves

In the field of plasma heating and current drive more than 20 experimental papers were presented. About half of them dealt with ECW-physics. A quarter dealt with ICH and IBW and one quarter with LH waves.

4.1 Electron Cyclotron Waves

The Swiss tokamak TCV [16] has the most flexible ECW-system as shown in FIG. 14. Together with the extensive shaping facilities TCV is well geared for fundamental tokamak research. Various achievements have been reported to the conference. Most noticeable is the scenario with complete ECCD to maintain the current. See FIG.15. The X3 facility allows heating at high density. Due to the long vertical chord of the beam along the HFS of the D-shaped plasmas the single pass absorption is as high as 70%. See FIG. 16.For this accurate feedback control of the launcher position is of advantage [17].

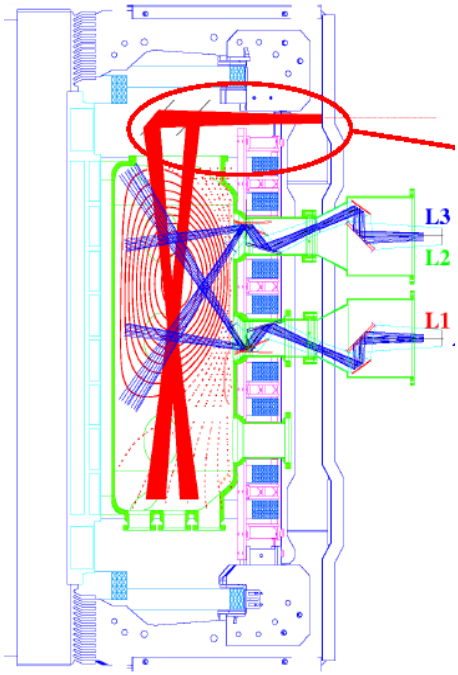

FIG. 14. The ECRH system at TCV [16]: in blue the microwave beams of the 82.7 GHz system with nominal 3 MW, 2 s power for Heating and current drive at 2nd harmonic X-mode (X2); in red the 118 GHz beams with nominal 1.5 MW, 2 s power for 3rd harmonic heating (X3). All beams can be swept toroidally and poloidally over plasmacross-section.

Also well equipped with a 3 MW, 110GHz, ECW-system is JT-60U [19], which achieved a record ECW-energy of 10 MJ deposited in the plasma. During NCS-discharges created by off-axis LHCD or NBI record values of T_{e0} between 24 and 27 keV are observed due to an e-ITB coinciding with the negative shear region. See FIG. 17.

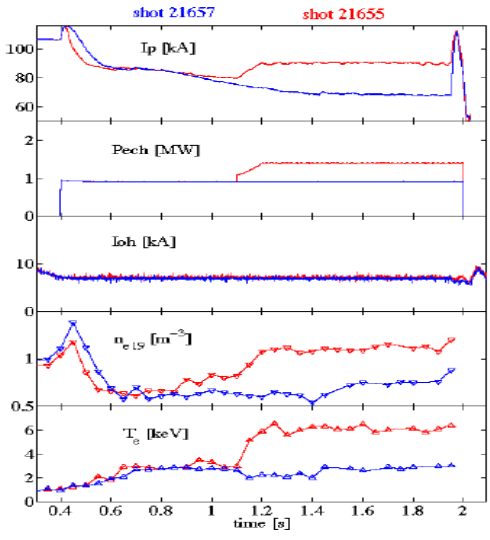

FIG. 15. A TCV plasma pulse with the current fully sustained by ECCD. In blue: a pulse with off-axis 0.9 MW Co-ECCD. In red: the changes if on-axis 0.45 MW Counter-ECCD is added. Stationary state for 4 current diffusion times [16].

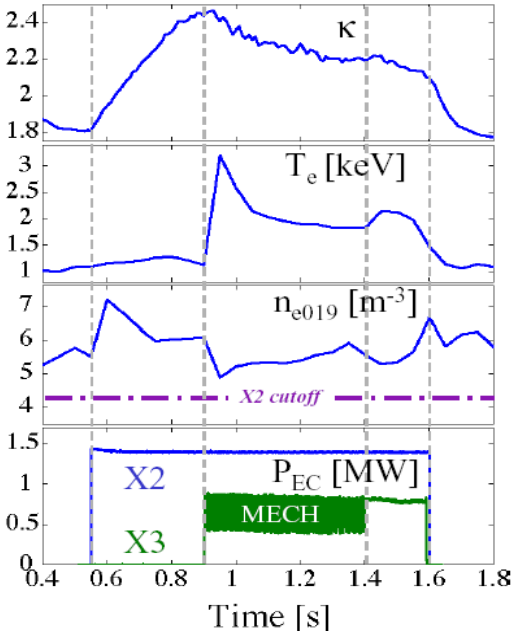

FIG. 16. The increase of T_e when X3-power is switched on with 70% single pass absorption during an off-axis X2 heated plasma in TCV [18].

The efficiency of ECCD has also been studied in JT60-U. See FIG. 18. Seemingly the experimental values are a bit lower than Fokker-Planck calculations predict.
In DIII-D [20] also ECCD efficiencies are measured. The normalized efficiency, which include a linear dependence on T_e increases when electron trapping effects are
reduced by either:
- Increasing β due to increasing electron density and/or temperature;
- Moving deposition towards inboard midplane;
- Moving deposition to a smaller minor radius.

All this in good agreement with CQL3D quasilinear Fokker-Planck code taking into account electron trapping as well as E_{par}. See FIG. 19.

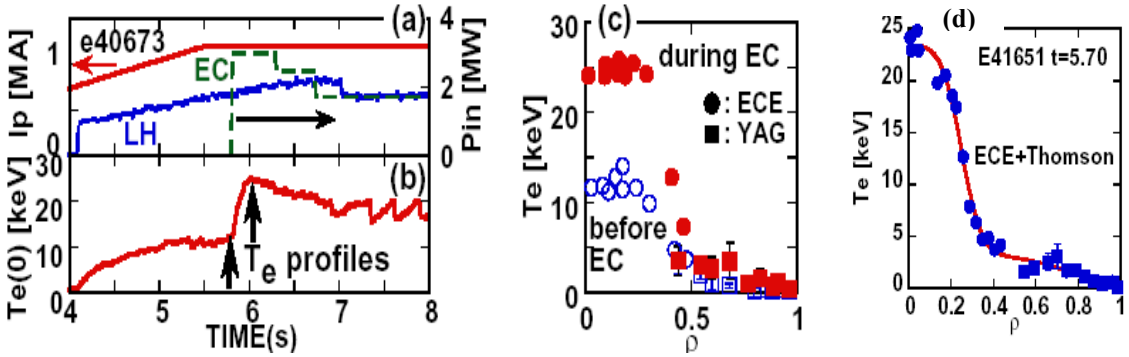

FIG. 17. Record values of T_{e0} obtained by 3 MW central ECRH in a NCS discharge of JT60-U (a, b). The profiles before and during ECH are given in (c). In (d) a result with NBI instead of LH [19].

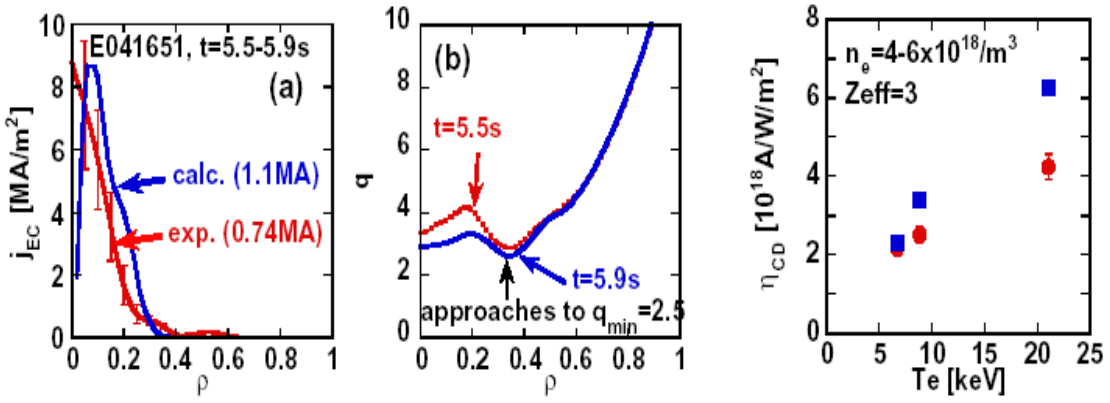

FIG. 18. ECCD experiments in JT-60U [19] (red) compared to the results of linearized Fokker-Planck calculations (blue). In (b) the q-profile at the beginning (red) and end (blue) of the calculation are given from which the parallel electric field is calculated needed for FP-calculations. The E_{par}-correction is not sufficient to explain why the efficiency (c) not increases linearly with T_{e0} but stays below predictions.

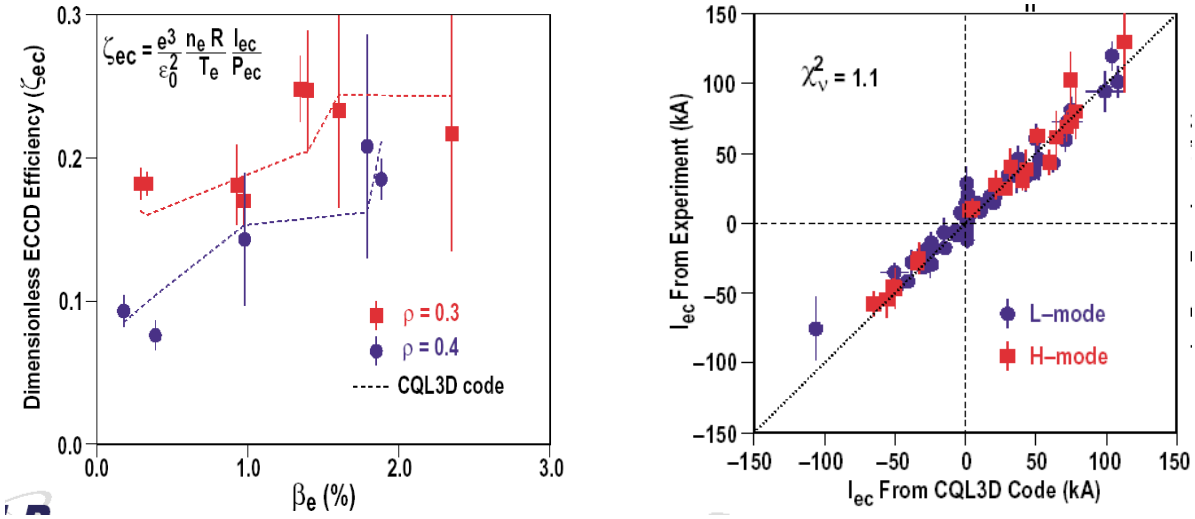

FIG. 19. The normalized current drive efficiency in DIII-D [20] compared to the predictions of the CQL3D-code: (a) as a function of β at 2 values of the deposition radius and (b) for all the simulations done

In TCV one included in CQL3D various transport coefficients for EC-heated fast electrons based on the observation of a very flat electron tail temperature profile by HXR-emissivity [16]. A diffusivity between 1.5 and 5.0 m2/s gave agreement with both the observed driven current and the HXR-observations. See FIG. 20. From this the TCV-team concluded that seemingly fast-electron transport does not differ much from thermal transport.

ECRH/ECCD has been proven to be able to stabilize 3/2 as well as 2/1 NTM in many machines like ASDEX-U [5], DIII-D [20] See also FIG. 31 in par.5.
Sawteeth stabilization has been shown in ASDEX-U [5], TEXTOR [11] and TCV [18].

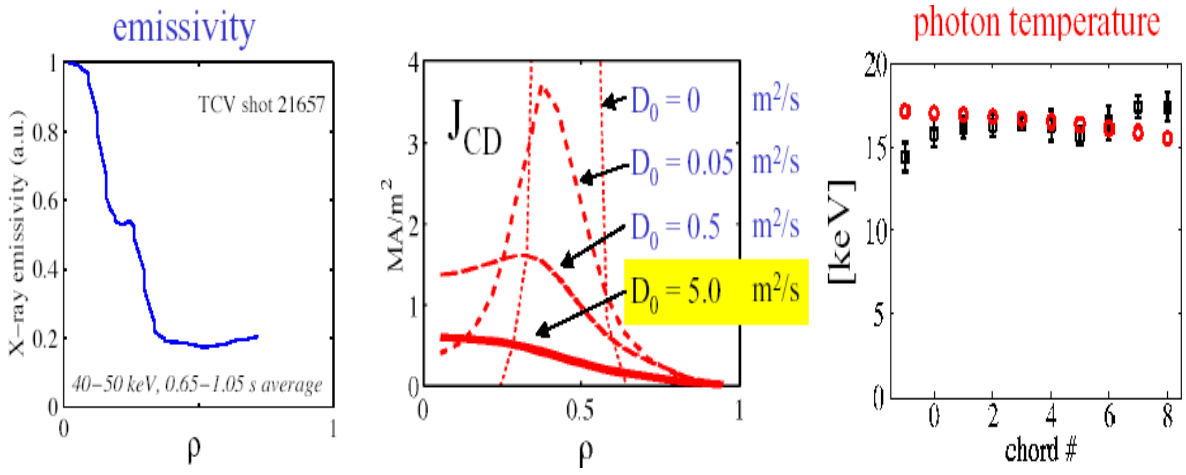

FIG. 20. The HXR-emissivity profile (left) in TCV [16] during ECCD. Inclusion of a diffusivity of 5 m2/s in CQL3D (mid) for fast electrons gives agreement with both the experimental value of driven current as well as the correct HXR- emissivity and photon temperature (right).

4.2 Electron Bernstein Waves

Electron Bernstein Wave heating has been successfully demonstrated in W7-AS [21] and NSTX [22].
In W7-AS it allowed to heat with 70 GHz in O-mode overdense plasmas (>10^{20}m^{-3}). See FIG. 21.

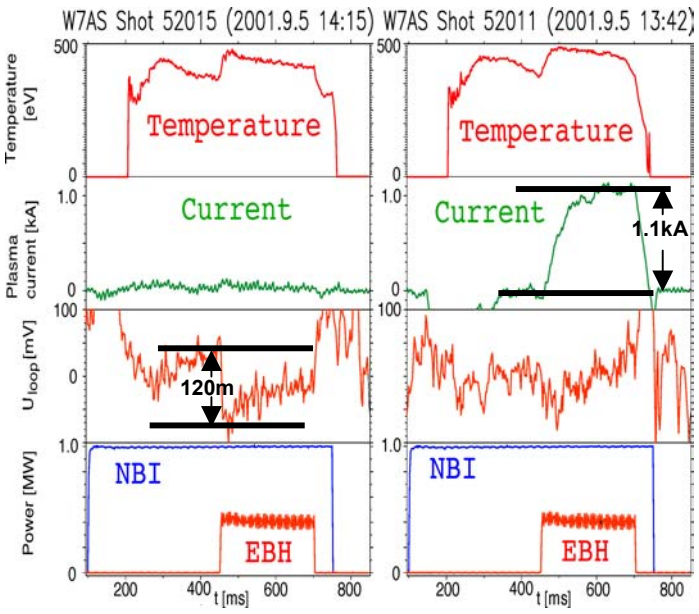

FIG. 21. EBWH in W7-AS [21] with 0.4 MW 70 GHz O-mode at n_e= 10^{20} m^{-3}; Z_{eff}= 1.5 B=2.15 T with (left) and without (right) enforcing current zero.

In NSTX at the very high β of 20-40% the X-mode cut-off and EBW conversion layers are only millimetres apart so the fast X-mode with frequencies around 10 GHz can tunnel to the EBW-branch. See FIG. 22.

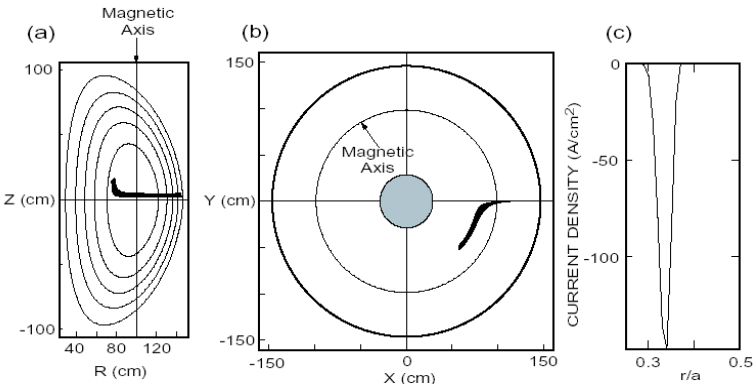

FIG. 22. Ray-tracing results of 14.5 GHz EBW in X-mode in NSTX [22] for β = 20%, n_e=3.10^{19}m-3 and T_{eo}=1 keV. The CD (right) is for 1 MW.

4.3 Ion Cyclotron waves and Ion Bernstein Waves

Ion Cyclotron Wave Heating is a well-established heating technique. Nevertheless new physics results were obtained at JET [23]:
- ICRH exerts toroidal momentum on the plasma such that off-axis heating both on HFS and LFS created hollow profiles of the toroidal rotation velocity;
- Mode conversion ^{4}He-^{3}He gives localized electron heating in good agreement with theory. See FIG. 23;
- Sawteeth control by ICRH deposition around the q=1 surface made it possible to avoid NTMs by control of the 'seeding' power of the sawteeth;
- Fast ions in the MeV-range have been created by 3ω_{ci} heating of plasmas with beam- of ^{4}He, which could be used for simulations of alpha particle heating and' burn control' (see FIG. 23);
- Transport of fast ions for these 'burn control' experiments could be modified by ICRH induced pinch effect.

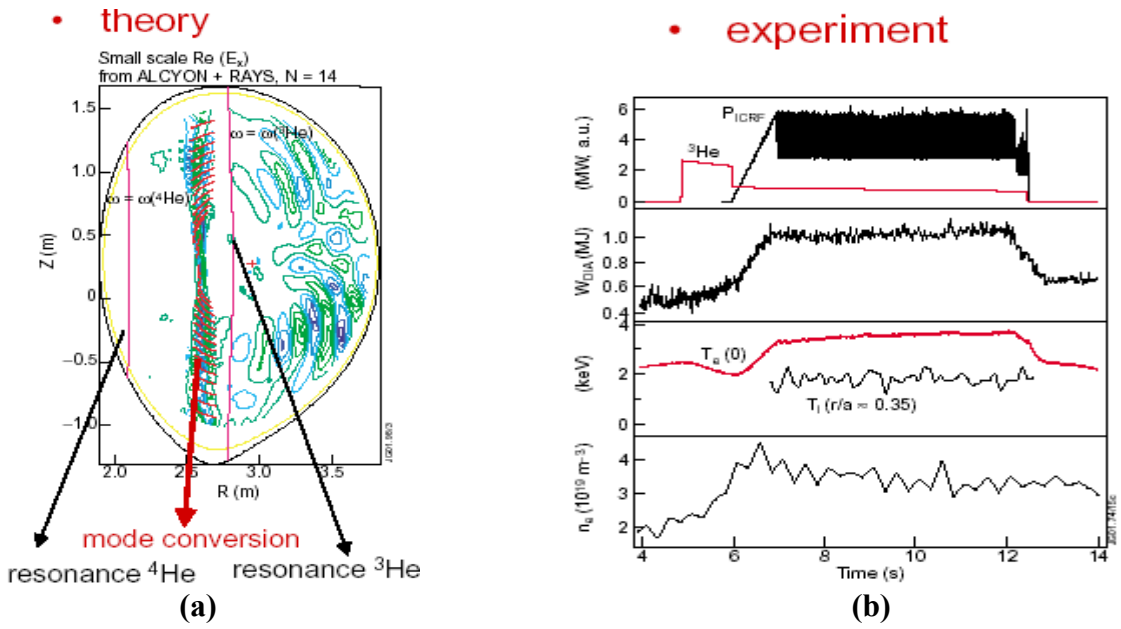

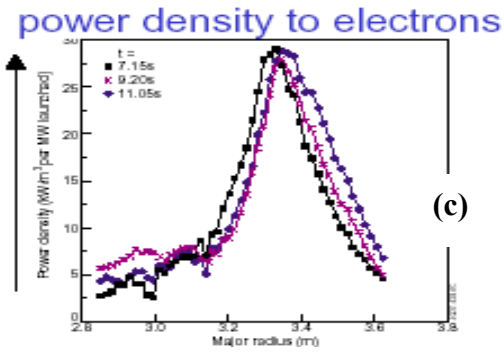

FIG. 23. Mode conversion ^{4}He-^{3}He in JET [23] gives localized electron heating.(a) Theory; (b)Experimental results.
On the right (c) the profile of the power deposition to the electrons.

Another interesting development is the High Harmonic Fast Wave heating on NSTX [24]. These experiments have demonstrated strong electron heating over a wide range of wave phase velocity (i.e. antenna array phasing). $T_e(0)$ increases up to 3.7 keV. See FIG. 24. H-mode could be achieved in D and He plasmas with RF alone. Loopvoltage differences between co- and counter-current-drive array phasing are indicative of RF-driven non-inductive currents. Also has been demonstrated that HHFW interacts with injected neutral beam ions such that a fast ion tail is produced.

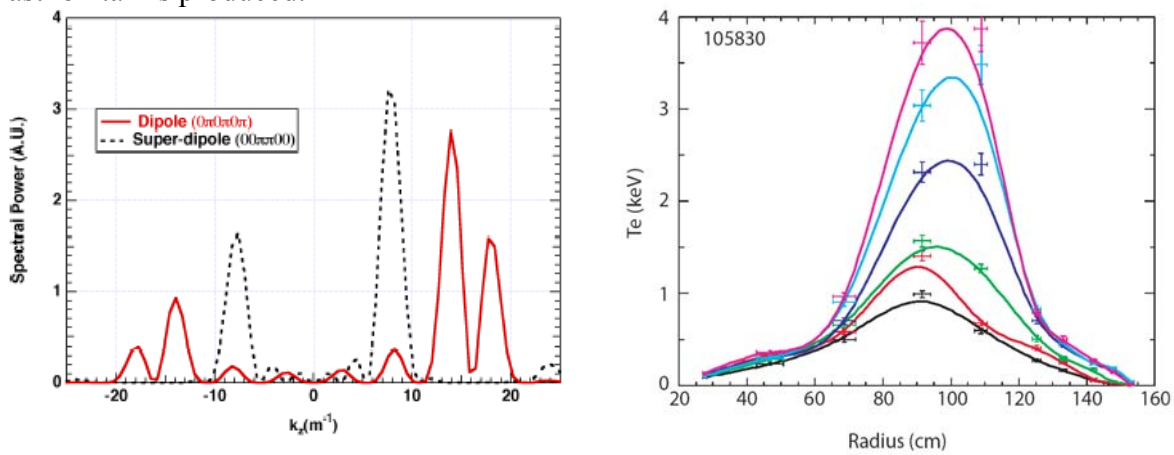

FIG. 24. The mode spectrum of the HHFW-system in NSTX [24] (left). The temperature evolution (right) due to strong electron heating by 2.7 MW of HHFW at 30 MHz. Density: 2.10^{19}m^{-3}, I_p=0.8MA, B_t= 0.45 T. The black curve is the ohmic temperature profile. The maximum temperature is reached after 100ms. A clear e-ITB is formed at half radius.

Ion Bernstein wave heating has been studied in several machines C-MOD, FTU and HT-7.
In C-MOD [8] mode conversion from IBW to slow wave ICW as predicted by [25] has been observed for the first time.
The Chinese HT-7 [27]. uses frequencies around 30 MW with B=1.8-2.0 T. Strong electron heating was observed due to electron Landau damping. With 200 kW a doubling of temperature (from 1.2 keV (ohmic) to 2.3 keV) and of the energy content was obtained. Synergy between IBW and LHCD was shown.
A similar scenario in FTU [26] lead to an increase of the energy content with a factor 1.5 above Ohmic with a IBW-power comparable to Ohmic power. See FIG. 25.

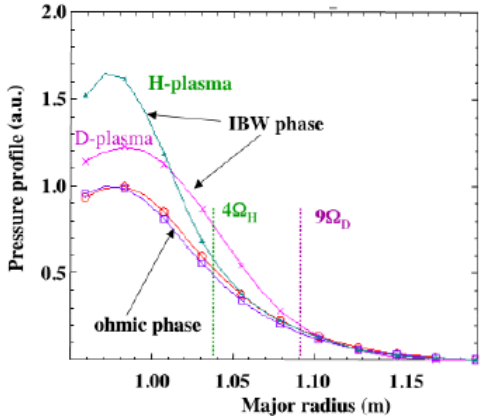

FIG. 25. IBW-heating in FTU [26] at 0.4 MA/ 7.9 T. A few hundred kW of IBWH gave a rise in the thermal energy content of 1.5 in D- and H-plasmas.

4.4 Lower Hybrid Waves

Lower Hybrid Current Drive has become one of the major tools to create central low or negative shear for AT-scenarios in many machines: JT60-U, JET, TS, C-MOD, FTU, TRIAM a.o. In JET much progress has been made in increasing the capabilities [23] of the LH-system by 2 methods: careful shaping of the LCFS near the grill-mouth and by CD_4 gas puffing. Also synergy with other heating methods lead to interesting results, which will be described in par.5 on integrated feedback control. In the last 2 years 1406 plasma pulses of JET with LHCD were used to study ITBs in AT-scenarios.
In TRIAM [28] LHCD was used together with ECRH. The team achieved a zero loop voltage plasma ramp-up scenario at a relatively high density, up to 2.10^{19}m-3. Preionisation by about 150 kW ECRH at 170 GHz (Bt-6-6.7 T) was followed by a LHCD-pulse of typically 100 kW at 8.2 GHz. The current ramp rate increased with LH-power. TRIAM held already the record pulse duration. This is extended now to 3 hours and 10 minutes with only 10 kW LHCD at 2.45 GHz.

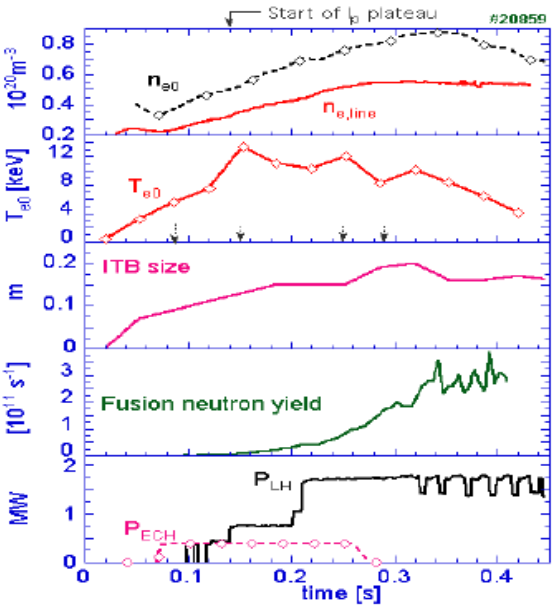

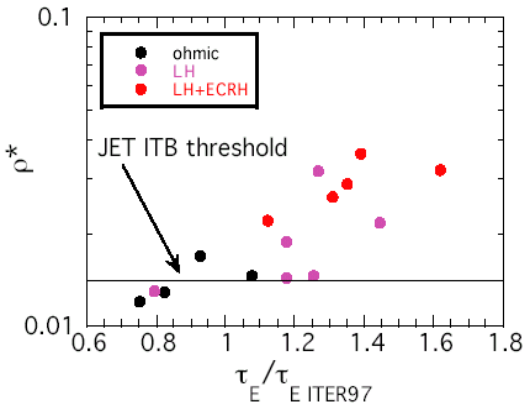

FIG. 26. An e-ITB in FTU [26] arises during combined EC + LHCD at high density. The e-ITB remains after EC switch-off .The increase in confinement goes together with the excess over the critical ρ for ITB-formation found at JET.*

Interesting is the observed synergy between ECRH and LHCD when at a given n_e= 1.3.10^{19} m^{-3} the EC-power is higher than 95 kW a sudden transition takes place with a marked increase in CD-efficiency as well as in confinement. This may be due to the formation of an e-ITB.
This is the explanation by a similar scenario in FTU [26] in which one obtained an e-ITB during 10 confinement times at the high density of n_e around 8.10^{19} m^{-3}. See FIG. 26. The increase in confinement above ITER97-scaling starts when the critical ρ* for ITB-formation as established by the JET-team is exceeded.

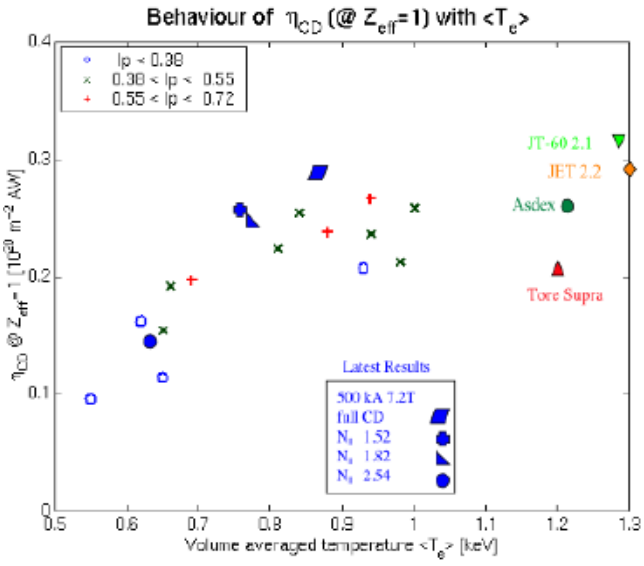

FIG. 27. LHCD current drive efficiency in FTU [26] as function of the volume averaged electron temperature compared with values of other machines

Zero loopvoltage combined with high density (10^{20} m^{-3}) has been demonstrated in FTU. The CD-efficiency increases with T_e up to 3.10^{19} $AW^{-1}m^{-2}$ until it saturates at that level. (FIG. 27)
The long pulses made possible by LHCD in TS will be described in the next paragraph.

5. Control issues

Control of plasma instabilities, like sawteeth and tearing modes by local heating is well established. An example is shown in FIG. 28 of profile control in TEXTOR [11] by ECRH leading to stabilisation of sawteeth. This was done by a pre-programmed choice of deposition radius. However one of the striking developments in plasma engineering in order to control the plasma is the widespread use of feedback systems. On previous conferences the one-to-one feedback control of one diagnostic signal as sensor and one actuator has often been shown. New on this conference was the demonstration of simultaneous feedback control of many quantities. See FIG. 29 of an example in JET [3], [14].

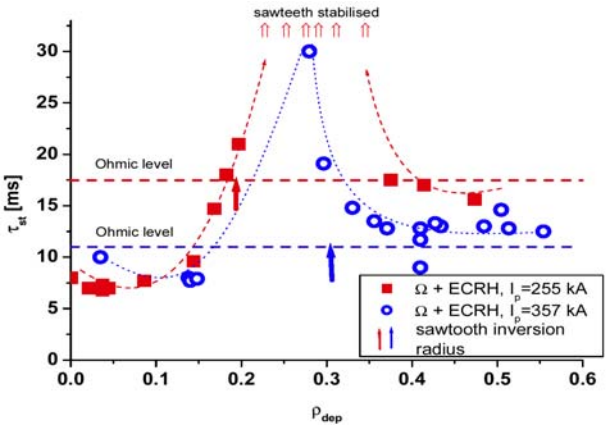

FIG.28. Sawtooth stabilization in TEXTOR by ECRH by positioning the ECRH deposition just outside the inversion radius [11].

The 4 minutes pulses in Tore Supra [29] are only made possible by simultaneous feedback control on density and current. See FIG. 30. Interesting new physics arises due to the non-linear behaviour of the plasma in response to the feedback circuits.
In Tore Supra slow oscillations (8 Hz) in the electron temperature can come up after 1 minute of zero loopvoltage operation. Tentative explanations say that probably a very central

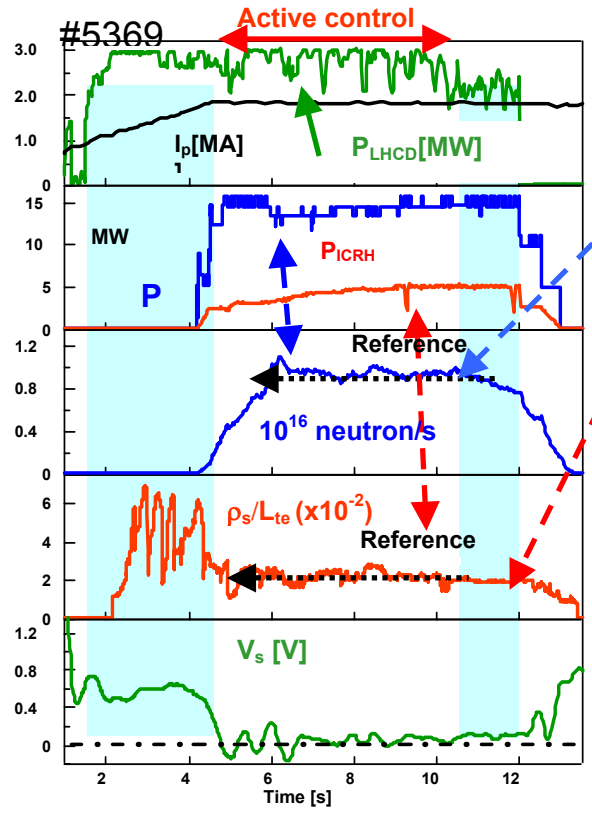

FIG. 30. The record duration pulse of Tore Supra [29] made possible by integrated feedback.

FIG. 29. An example of combined feedback action in JET:

Currentdensity profile control by LHCD

neutron rate controlled by NB

T_e-profile controlled by ICRH

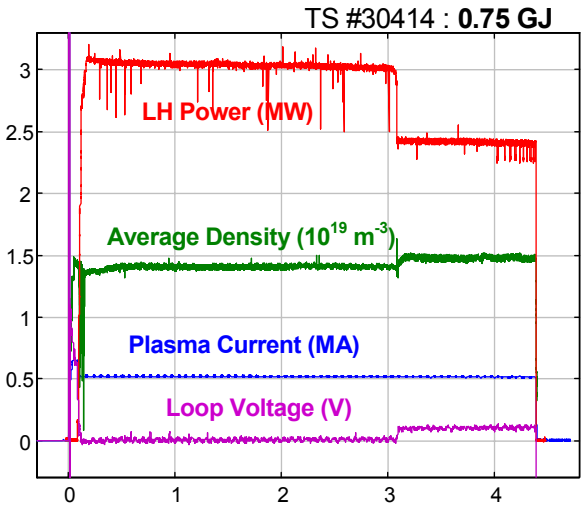

ITB is formed which influences the current-distribution. The counteraction of the current feedback is such that the ITB disappears until the next cycle. See FIG.31.

FIG. 31. Temperature oscillations in Tore Supra [29] due to non-linear plasma behaviour in conjunction with feedback control.

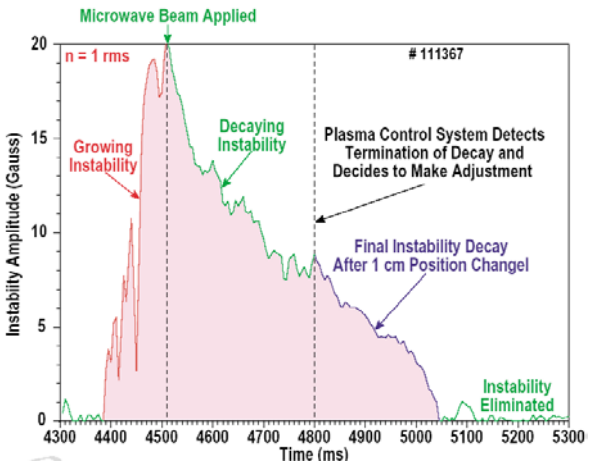

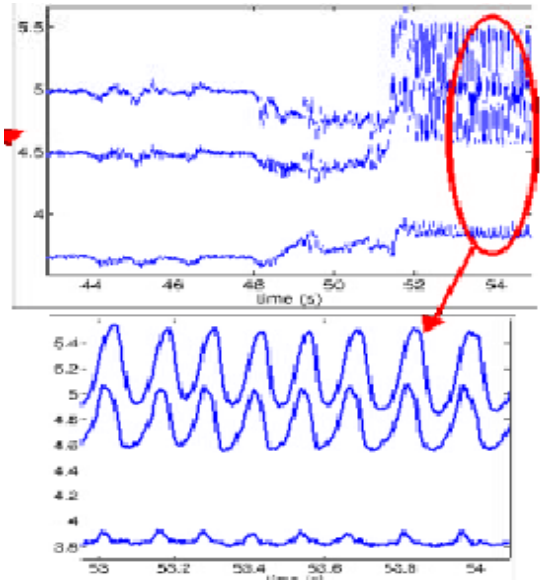

Feedback control on 2/1 NTM-mode in DIII-D [20] by combined action of ECW and plasma positioning is shown in FIG. 32.

FIG. 32. Control of the 2/1 NTM by ECRH and position control in DIII-D [20].

The concerted actions of heating, fuelling and exhaust systems under integrated feedback control have enabled reaching steady state conditions that were inaccessible in the past.
The tight feedback control of parameters makes it easier to clarify what is the cause of what. Therefore it is already clear now that *feedback systems* will fully dominate the operation of ITER.

6. Spherical Tokamaks

The family of spherical tokamaks and spheromaks are characterized by their position on the diagram: Aspect ratio versus I_p/I_{tf} ratio. See FIG. 33 taken from [30]. The Spheromak SSPX and FRC-experiments in FIX will be discussed in another summary. In this paragraph only the reports on Spherical Tokamaks will be summarized: MAST, NSTX, Globus-M and Pegasus.

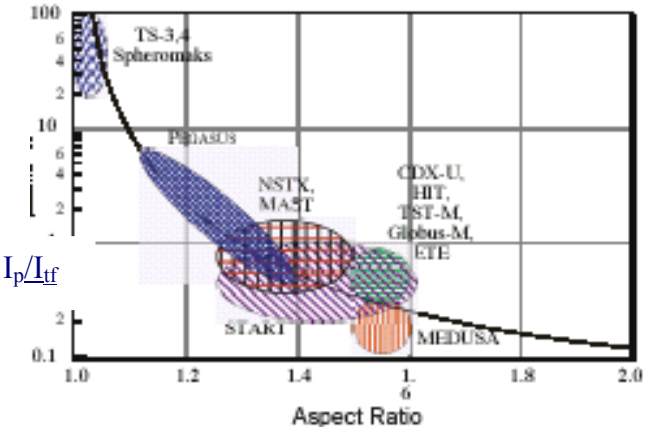

FIG. 33. The position of spherical tokamaks and spheromaks on the diagram [30] of Aspect Ratio versus I_p/I_{tf} ratio.

The low aspect ratio of MAST [31] allows differentiation between different forms of the H-mode threshold scaling. With optimized fuelling (inboard puffing) the H-mode power threshold data lie up to a factor 1.7 above recent scaling laws. Slight changes in the magnetic configuration of a connected Double Null Divertor (DND) over a distance in the order of the ion Larmor radius significantly influence H-mode access. H-mode confinement in discharges with low frequency ELMs is generally consistent with the IPB98(y,2) scaling. See FIG. 34.

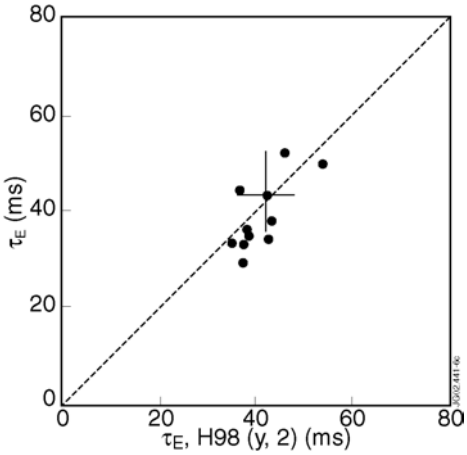

FIG.34. Confinement scaling of MAST [31] plasmas is in agreement with H98(y,2) predictions

Strong indications of both particle and energy internal transport barriers have been seen. Divertor power loading studies, including transient effects due to ELMs, show a strong bias of power efflux to the outboard targets. ELM energy losses, δW_{ELM}, are less than 4% of the stored energy in all regimes explored so far, but ELM effluxes extending 30cm outside the outboard separatrix have been measured. See FIG. 35.

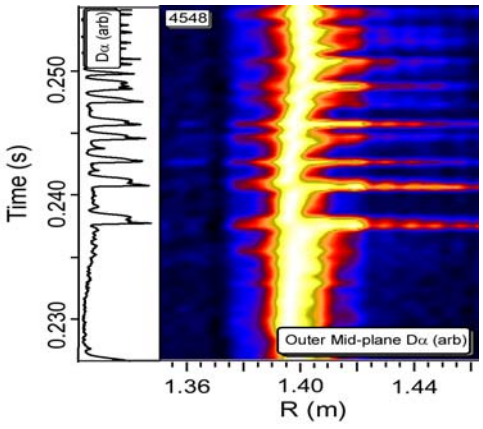

FIG. 35. The radial excursions of D_α-emission during ELMs in MAST [31].

β_N > 5 have been obtained in MAST, approaching the ideal n = 1 no wall external kink stability limit. However NTMs (3/2, 2/1) triggered by sawteeth have been observed to limit the β. In par.3 the existence of strong ITBs in MAST are already described.

In NSTX [32] research has been enabled by neutral beam (up to 7 MW) and high harmonic fast wave heating (up to 6 MW), toroidal fields up to 6 kG, plasma currents up to 1.5 MA, flexible shape control, and wall preparation techniques. These capabilities have enabled the generation of plasmas with $<\beta_T>$ up to 35%. β_N-values up to 6 can exceed the no wall limit with 30%, and studies suggest that passive wall mode stabilization is enabling this for broad pressure profiles characteristic of H mode plasmas. High bootstrap current fraction operations leading to 60% non-inductive current fraction has been established for ELMy H mode plasmas and sustained for several current relaxation times. The results with HHFW and EBW-heating have already been already described in par.4. See FIG. 24.

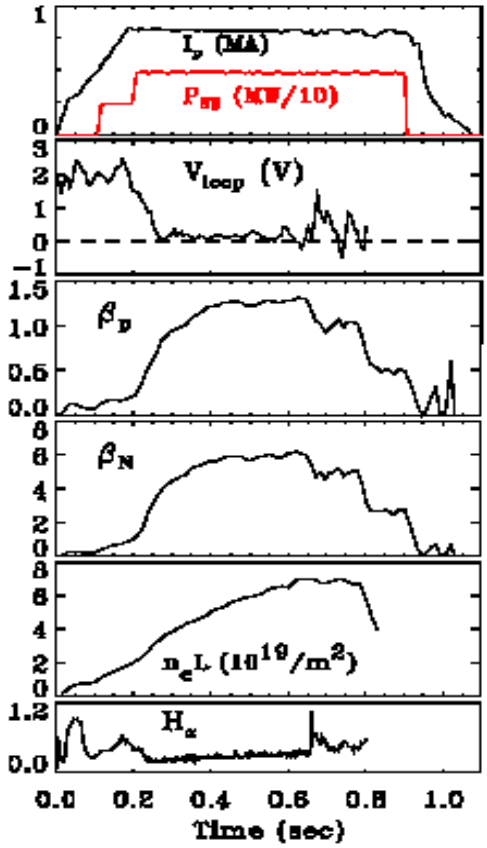

FIG. 36. One of the record high β pulses in NSTX [32] with 60% non-inductive current

Energy confinement in NSTX plasmas with both L- and H-mode edges exceed the ITER89 L-mode scaling respectively the ITER98(y,2) predictions. See FIG. 37. Also in NSTX, as in MAST [10], the power threshold for H-mode access appears to be significantly higher than predicted by the present-day scaling based on high aspect ratio machines [33]. The formation of strong ITBs has been already described in par.3.

The St.Petersburg spherical tokamak Globus-M [34] reported initial results of operation with currents up to 0.36 MA at Bt = 0.55 T. Fuelling by injection of plasma clusters allowed to reach densities up to 7.10^{19} m^{-3}.

The Wisconsin Pegasus Toroidal Experiment [30] is a mid-sized (R = 0.25 - 0.45 m) extremely low aspect ratio (A= 1.1 – 1.4) spherical torus (ST). It has the dual roles of

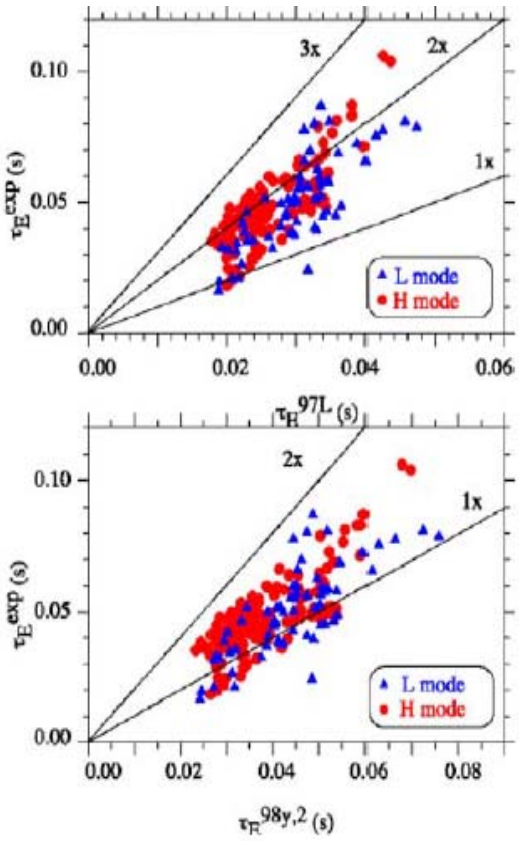

FIG. 37. Confinement in NSTX both for L- and H-mode exceeding the relevant ITER-scaling [33].

exploring limits of ST behavior as A approaches 1 and studying the physics of ST plasmas in the tokamak-spheromak overlap regime (I_p<= 0.15 MA, and B_T < 0.1 T). High beta plasmas are produced at very low toroidal field by ohmic heating. Values of β_T> 20% have been obtained. Achievable plasma current is subject to an apparent limit of I_p/I_{tf} ~1. Access to higher-current plasmas appears to be restricted by the appearance of large internal MHD activity, including m/n=2/1 and 3/2 modes. Recent experiments have begun to access ideal stability limits, with disruptions observed as q_{95} approaches 5.

7. Stellarators

Reports on the following stellarator devices were submitted during this conference:
LHD, W7-AS, CHS, TJ-II, Heliotron-J, H-1NF. This conference witnessed the breakthrough of LHD [35] as a major fusion relevant device as well as it had to say goodbye to a stellarator that had brought an enormous amount of knowledge in stellarator physics and plasma physics in general: W7-AS [36].
The LHD-team presented 12 papers to the conference next to their overview paper. These gave details of the record values in stellarator research obtained in 4 years of LHD-operation [35]. In the first place the record triple product: $nT\tau_E$ of $2.2 10^{19}$ m^{-3}.keV.s at τ_E = 0.36 s, $T_e(0)$=1.3 keV, n = 4.8 10^{19} m^{-3} . Other impressive values are:

- Maximum stored energy 1.2 MJ
- Maximum operational density $1.5.10^{20}$ m^{-3}
- Maximum electron temperature $T_e(0)$= 10 keV at n= 0.6 $10^{19}m^{-3}$;
- Maximum ion temperature $T_i(0)$= 5 keV at n= 0.7 $10^{19}m^{-3}$
- Maximum beta β = 3.2% at B = 0.5 T
- Discharge duration 127 s
- Input Power by: NBI 9MW, ICRH 2.7 MW, ECRH 1.9 MW.

These results were made possible by the suppression of neo-classical helical ripple transport with geometrical optimization: mainly by inward shift of magnetic axis. This gave good confinement down to ν* of 0.05. See FIG. 38.

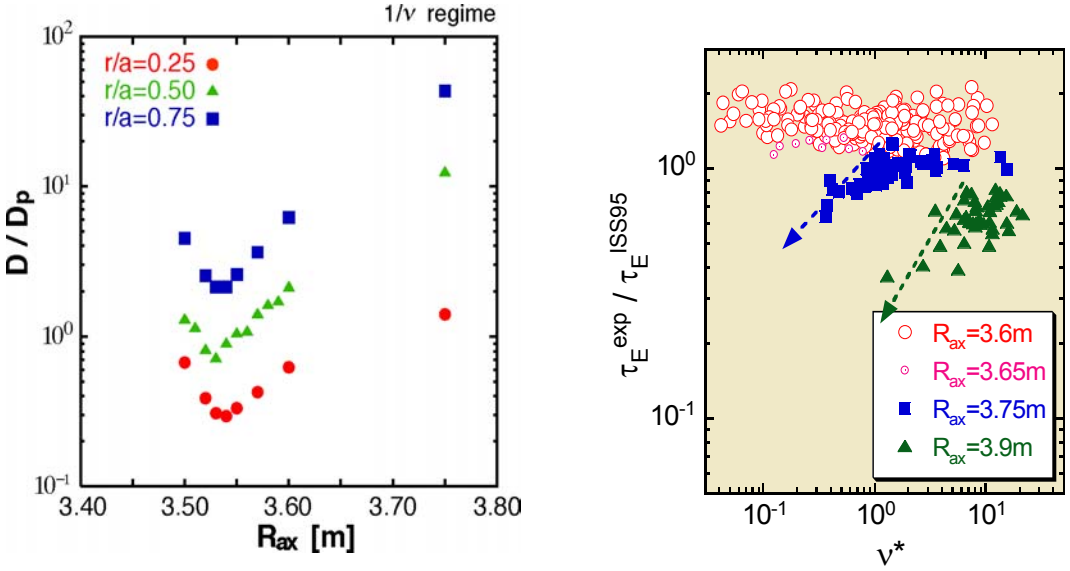

FIG. 38. The improvement confinement in LHD [35] obtained by shifting the magnetic axis inwards, which suppressed the neoclassical transport due to helical ripple

Other interesting transport findings of LHD:
- no profile stiffness;
- τ_E increases with $n_e^{0.6}$ up to maximum;
- continuation with pellet- ITB at rational iota-values;
- measurements of reduced χ_{eff} inside islands.

At the end of its operational lifetime W7-AS [36] achieved a major breakthrough by the introduction of the island divertor. See FIG. 39. This has made it possible to develop a new regime: High Density H-mode (HDH).

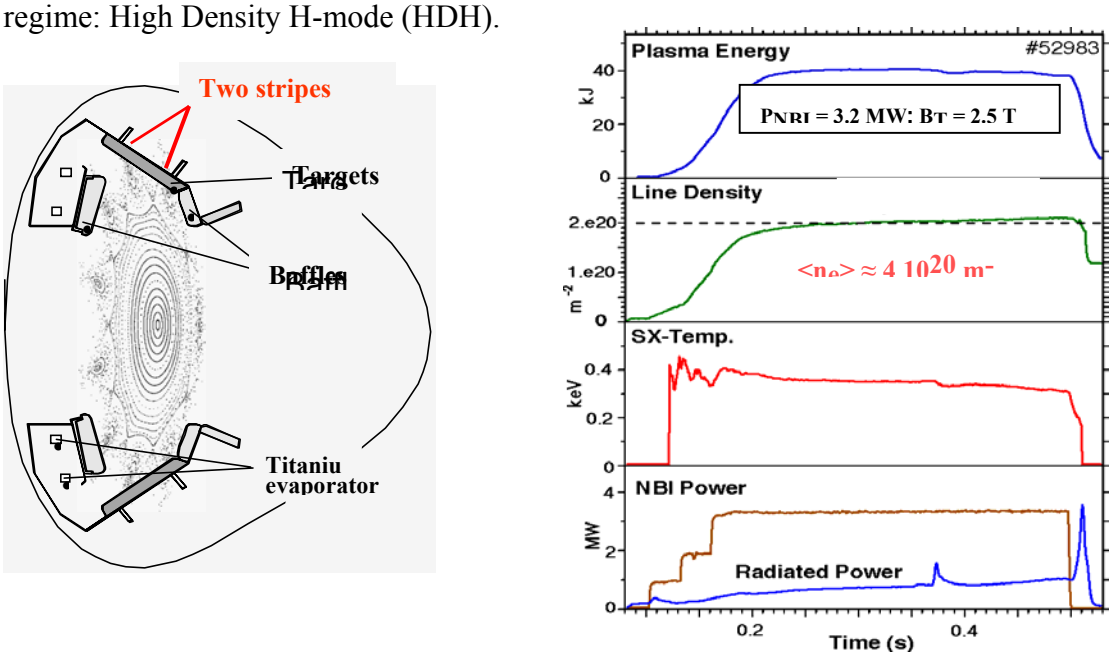

FIG. 39.a. The island divertor (right) of W7-AS [36] that made the HDH-regime possible with typical time-traces (right).

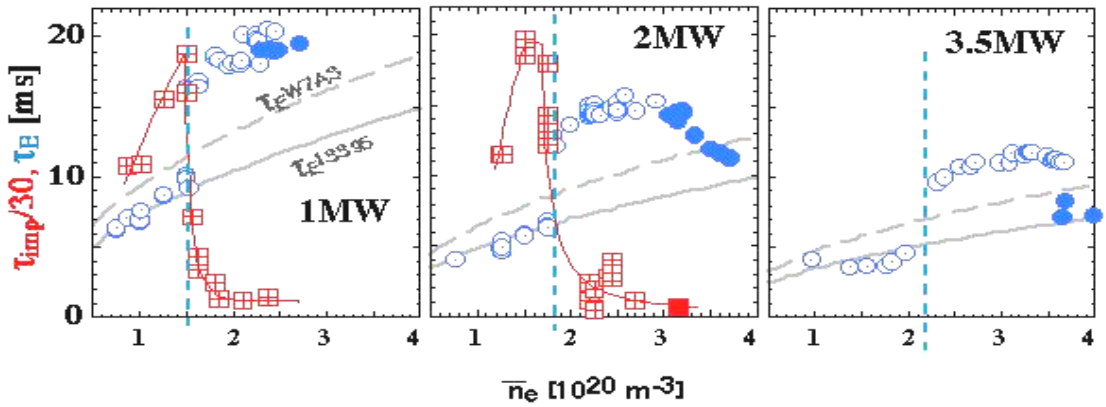

FIG. 39.b. The sudden change in confinement times when the HDH-mopde set in at $n_e > 1.5.10^{20}$ m^{-3}. Note the self-purification due to a dramatic decrease of τ_{imp}.

In this regime β of 3.2% has been reached with a line-averaged density of $4.5.10^{20}$ m^{-3}. Most noticeable of this regime is the self-purification: the impurity confinement time τ_I goes down with increasing τ_E. Other transport findings (outside HDH-mode):
- no profile stiffness;
- transport modified at rational iota values (ITBs).

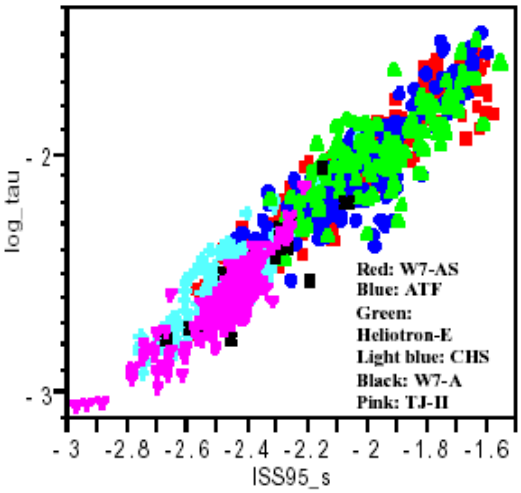

FIG. 40. The ISS-scaling of various stellarators. The pink values indicate the extension made by the TJ-II [37] values at extreme low q-values

Interesting results from TJ-II, CHS, Heliotron J and H-1 NF were reported confirming the validity of the ISS95-scaling. TJ-II [37] extended (see FIG. 40) the range in iota/q-values of this scaling confirming the dependence: $\tau_E \sim q^{-0.4}$ in the range q = 0.9 - 0.4 (previous device-values: q = 3 - 1). Low q-values were not restricted by stability (Note: the TJ-II-only database gives $\tau_E \sim q^{-0.5}$). Other TJ-II observations on transport:

- Negative shear gives confinement improvement;
- No improvement with positive shear;
- ITBs observed at q=2/3 with negative shear. See FIG. 41.

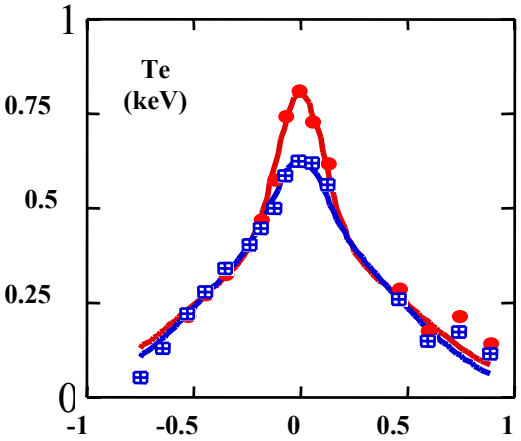

FIG. 41. The increase of T_e in TJ-II [37] within an e-ITB (red) at ρ=0.2 coinciding with the location of q=2/3 when that value enters the plasma compared to the profile (blue) just before that time.

8. Pinches

Research on pinches is nowadays focused on Reversed Field Pinches (RFP). Results of the following devices were reported to this conference: MST, RFX, EXTRAP, TPE-RX. Spheromak type pinches like SSPX and FRC's will be described in another summary.
Two major findings in RFP physics brought enthusiasm to the fusion community:
1. Pulsed poloidal current drive (PPCD) in the edge plasma of several RFP's gave impressive improvements of confinement most noticeable in MST [38].
2. Reduction of mode spectra to a Quasi Single Helicity mode showed very good confinement inside the main mode. Single helicity would be even better!
In FIGs.42.a and .b the principle of PPCD is explained. The results on confinement are spectacular. On MST [38] (see FIG. 42.b) one reached a ten-fold increase in τ_E to a value of 10 ms, β doubled to 15% and the central value of T_e increased with a factor 3 to a value of 1.3 keV. Altogether the MST-team claimed tokamak-like confinement. An important issue in the RFP-community is however the question if this promising plasma state can be made stationary. After all the duration at MST was just one confinement time. Advocates propose RF-current drive for maintaining the optimum current-density distribution instead of PPCD. This could enable to achieve long periods whilst PPCD has by definition a finite duration. If this can be proven to be possible in the future the RFP-concept (if one can still call this configuration as such) may become a serious alternative road to a fusion reactor.

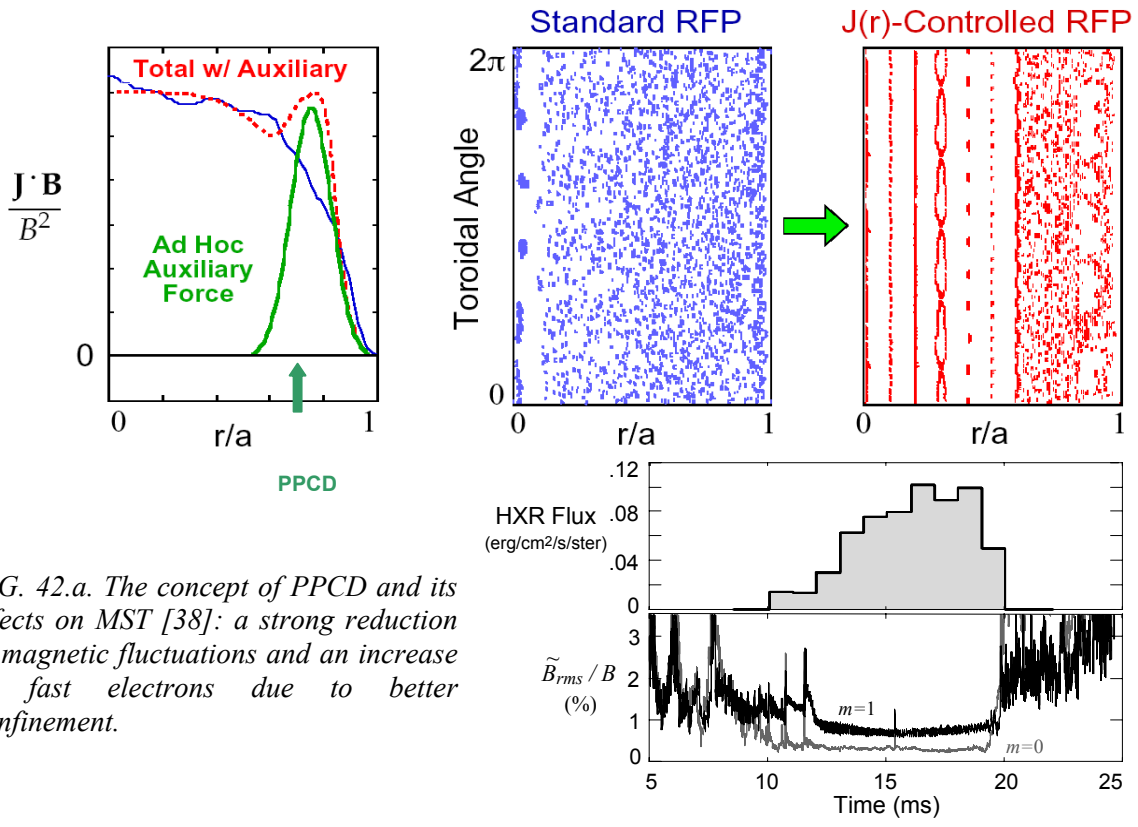

FIG. 42.a. The concept of PPCD and its effects on MST [38]: a strong reduction in magnetic fluctuations and an increase in fast electrons due to better confinement.

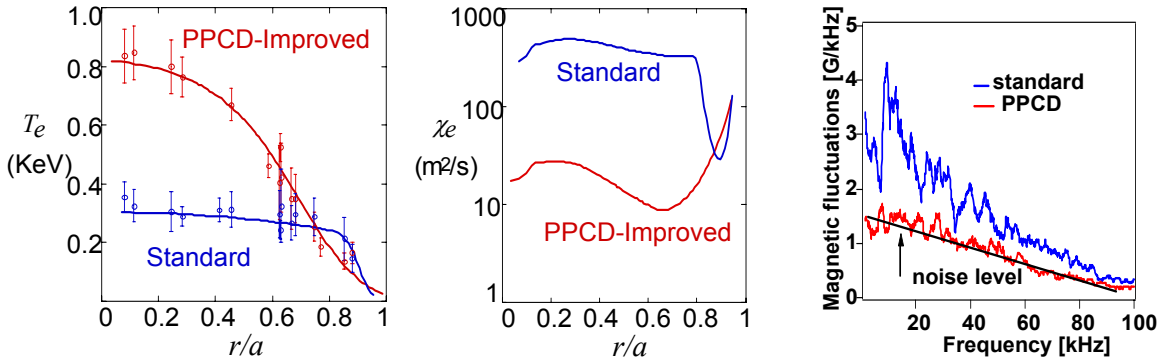

FIG. 42.b. Further results of PPCD in MST [38]; the increase in T_e, the reduction of χ_e and the reduced spectrum of fluctuations.

Single Helicity (SH) is a laminar self-organized RFP state with a unique *m*=1 saturated resistive kink. See FIG. 43. SH has good helical flux surfaces, with a significant *magnetic well* in the plasma core. Simulations show a large decrease of transport in SH with respect to standard RFP [39]. Experimentally robust Quasi Single Helicity spectra are observed in all major RFP devices (RFX, EXTRAP, MST, TPE-RX):

- one *m*=1 kink dominates;
- secondary m=1 modes still have non-zero amplitude;
- a coherent and hotter helical structure emerges;
- confinement improves with reduction of secondary modes (QSH↔SH).

Therefore SH is regarded as an approach to improve confinement in a steady state RFP. Complementary to active control of magnetic turbulence also an increase of the volume inside the SH-mode relative to the total plasma volume is required.

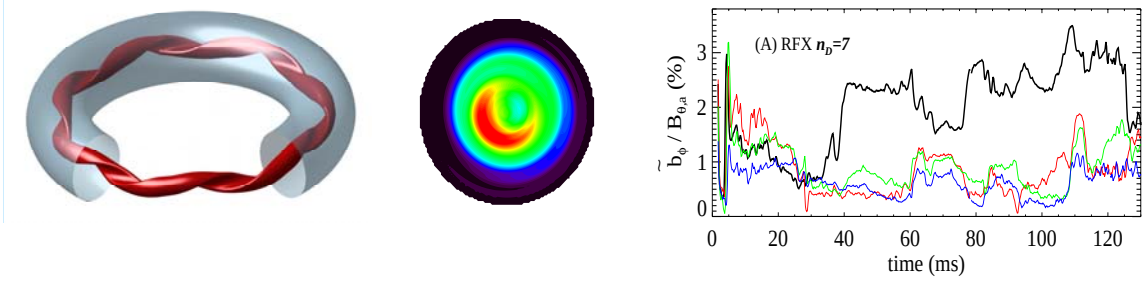

(a) **(b)** **(c)**

FIG. 43. (a) The topology of the Single Helicity mode [39]; (b) An experimental reconstruction of the QSH-mode in MST [38]; (c) An example of the magnetic field of the main mode (black) in RFX [39] and the secondary modes (coloured).

9. Mirrors

Experimental Mirror studies at 5 devices were presented. In Japan there is GAMMA-10 [40], in Russia [41] GDT, GOL-3 and AMBAL-M and in Korea HANBIT [42].

Potential formation physics and potential confinement effects along B-field are theoretically proposed and experimentally verified in *GAMMA-10 tandem mirror*. This scaling of the potential and its formation with ECH power and plasma parameters provides a future roadmap for *GAMMA 10*: (a) *the high-potential mode* and (b) *the hot-ion mode*. The results of the latter mode are very promising with T_i=10-20 keV, n_e= 4.10^{18} m^{-3} , τ_E= 10 ms and thermal fusion neutrons in agreement with the measured ion temperature.

The Russian ambipolar trap *AMBAL-M tandem mirror* reported that high ß plasmas ~40% are stably confined at densities up to n_c=6. 10^{19} m^{-3} . Also in the simple *GDT mirror* with a 7 m long central cell ß-values close to unity could be achieved with n_c~4. 10^{19} m^{-3}.
Even more open is *the GOL-III multi-mirror* with a corrugated axial magnetic field around 5 T and 2 end mirrors with a mirror ratio of only 2. In this device high density plasmas (~10^{21} m^{-3}) were heated up T_e ~2 keV with a Relativistic Electron Beam (REB). The longitudinal electron heat conduction, if it had been collisional, would have been excessive and would have prevented such high temperatures and densities. The group explains this interesting result by a 1000-fold increase in the effective electron collision frequency due to REB-induced micro turbulence.
In Korea *the HANBIT tandem mirror* came into operation and demonstrated plasma heating with ICRH. In general one can say that the mirror-concept studies showed progress and should not be forgotten in the efforts to achieve a fusion reactor albeit that this concept maybe more useful for a neutron material test facility than for a reactor. It should be noted that not many concepts can claim a plasma confinement with no anomalous diffusion as has been reported for plasmas in: (a) GDT; (b) AMBAL-M (D^ ~10^{-1} m^2 /s) and (c) the high-potential mode of GAMMA-10 (D around 0.06 m^2/s)

10. Conclusions

10.1 General conclusions

1. Several experimental teams have proven that the *ITER physics requirements* in dimensionless form are close to be met simultaneously in present-day machines.Therefore we can ask the authorities with confidence to allocate the resources to build ITER. The chances that the project will reach its goals are high.

2. Operation in so-called '*Advanced Tokamak Scenarios'* with very low or negative central shear has reached maturity and has been proven to be a competing alternative to standard ITER-scenarios

3. There is a quickly growing reliance on *feedback systems* to harness unruly plasmas by *concerted actions of heating, fuelling and exhaust systems:*
- It allows us to reach steady state conditions that were inaccessible in the past;
- The tight control of parameters by feedback action makes it easier to clarify what is the cause of what;
- Therefore it is clear that *feedback systems* will fully dominate the operation of ITER.

10.2 Conclusions on Confinement

1. Turbulent transport of hot plasmas continues to confront us with unsolved questions but some aspects become more clear:
- *drift-wave turbulence* is an important if not dominating ingredient. This follows indirectly from comparison between measured and predicted profiles. Now also a more direct proof has been given by comparing correlation length and times;
- *electromagnetic effects and MHD induced turbulence* do play an important role as well in particular at high beta.

2. Major riddles in confinement remain to be solved:
- ITBs
- Non-local effects
- Inward convection
- Island induced transport

3. There are many similarities between turbulent phenomena in quite different magnetic confinement schemes as tokamaks, stellarators, RFPs.

10.3 Conclusions on Alternative Concepts

1. The case of the *Stellarator* concept as an independent route to a fusion reactor has been strengthened (statement of F.Wagner on this conference) as follows from:
- Performance being close to tokamak achievements at comparable dimensions;
- The understanding of neoclassical versus anomalous transport.

2. Important progress has been made in *RFP* physics:
- Tokamak-like confinement times has been reached albeit transiently;
- The influence of helical modes and their spectrum with single helicity giving important confinement improvement.

3. Progress in *Mirror* achievements:
- high ß achieved up to 40%.
- confinement times in the ms-range.

4. *Small tokamaks* (although not discussed in this summary) are important for:
- education of a new generation of fusion physicists and engineers
- spreading of knowledge on fusion outside the industrialized world.

Caveat:

The author apologizes for the limited extent of this summary. The more than 120 contributions that should be covered could not be represented fairly in the limited space and time allocated to this summary. The author realizes that no justice is done to many very good papers and that his choice of what to mention or not shows arbitrariness.

Acknowledgements

This work has been made possible by support from the Association Euratom-FOM with financial contributions by the Dutch Organisation for Scientific Research NWO and the IAEA.

References:

[1] K. Razumova, "Stability, Current Drive and Heating, Energetic Particles; a summary review". Proc.18th IAEA Fusion Energy Conference, Sorrento, Italy 2000.
[2] T.Fujita et al., "Overview of JT-60U Results toward High Integrated Performance in Reactor-relevant Regime, Paper OV/1-3. This conference.
[3] J.Pamela et al.,"Overview of JET results", Paper OV/1-4, This conference.
[4] K.Burrell et al., "Overview of Recent Experimental Results from the DIII-D Advanced Tokamak Program", Paper OV/1-5. This conference.
[5] H.Zohm et al., "Overview of ASDEX Upgrade Results", Paper OV/2-1, This conference.
[6] G.R. McKee et al., "Turbulence Regulation and Stabilization by Equilibrium and Zonal Flows" Paper EX/C4-1Ra. This conference. And
T.L.Rhodes et al., "Quantitative Comparisons of DIII-D Turbulence Measurements to Gyro-Kinetic and Gyro-Fluid Turbulence Simulations", Paper EX/C4-1Rb. This conference.
[7] F.Ryter et al., "Electron Heat Transport in ASDEX Upgrade: Experiment and Modelling", Paper EX/C4-2Ra. This conference
[8] E.S.Marmar et al., "Overview of Recent Alcator C-Mod Research", paperOV/4-1. This conference
[9] S.Cirant et al., "Experiments on electron temperature profile resilience in FTU tokamak with continuous and modulated ECRH", paper EX/C4-2Rb. This conference.
[10] P.G.Carolan et al., "H-mode access physics in MAST", paper EX/C2-6. This conference.
[11] F.C.Schüller et al., "Overview of TEXTOR Results", paper EX/P5-13. This conference
[12] R.Brakel, "Electron Energy Transport in the Presence of Rational Surfaces in the W7-AS Stellarator", Nucl.Fusion 42, 903, 2002.
[13] E.H.Joffrin et al., "Internal Transport Barrier Triggering by rational magnetic flux surfaces in tokamaks", paper EX/P1-13. This conference

[14] X.Litaudon et al., “Progress towards steady-state operation and real time control of Internal Transport Barriers in JET, paper EX/C3-4. This conference
[15] D.Mazon et al., “real-time Control of Internal Transport Barriers in JET”, Plasm.Phys.Contr.Fusion 44, 1087, 2002
[16] T.P.Goodman et al., “Control of the Sawtooth Instability by Electron Cyclotron Heating and Current Drive In the TCV and ASDEX Upgrade Tokamaks”, paper OV/4-2. This conference.
[17] L.Porte et al., ” Third Harmonic X-mode Electron Cyclotron Resonance Heating on TCV using Top and Low Field Side Launch”, paper EX/P5-15. This conference.
[18] A.Pochelon et al., “Optimisation of Current Profile Using Far Off-axis ECH Power Deposition to Extend High Elongation Operation in TCV”, paper EX/P5-14. This conference.
[19] T.Suzuki et al., “Heating and Current Drive by Electron Cyclotron Waves in JT-60U”, paper EX/W-2. This conference.
[20] C.C.Petty et al., “Physics of Electron Cyclotron Current Drive on DIII-D”, paper EX/W-4. This conference.
[21] V.Erckmann et al., “ECRH at W7-AS”, paper EX/W-3. This conference.
[22] P.C.Efthimion et al., “Application of Electron Bernstein Wave Heating and Current Drive to High Beta Plasmas”, paper EX/P2-12. This conference.
[23] J.-M.Noterdaeme et al., “Heating, current drive and energetic particles studies on JET in preparation of ITER operation”, paper EX/W-1. This conference.
[24] P.M.Ryan et al, “RF Heating and Current Drive on NSTX With High Harmonic Fast Waves”, paper EX/P2-13. This conference.
[25] F.W.Perkins, “Heating Tokamaks via the Ion-Cyclotron and Ion-Ion Hybrid Resonance”, Nucl.Fusion 42, 1197, 1977
[26] F.Romanelli et al., “Overview of the FTU Results”, paper OV/4-5. This conference
[27] J.Li et al., “Integration of the High Performance Discharges toward Steady-State Operation in the HT-7 Tokamak”, paper OV/5-1. This conference.
[28], H.Zushi et al., “Overview of steady state tokamak plasma experiments on TRIAM-1M, paper OV/4-6. This conference.
[29] J.G.Jacquinot et al., “Recent developments towards steady state physics and technology of tokamaks in Cadarache”, paper OV1-2. This conference.
[30] R.J.Fonck et al., “Performance and Stability Limits at Near-Unity Aspect Ratio in the Pegasus Toroidal Experiment”, paper EXP3-09. This conference
[31] B.Lloyd et al., “Overview of Recent Experimental Results on MAST”, paper OV/2-3. This conference
[32] E.J.Synakowski et al., “The National Spherical Torus Experiment (NSTX) Research Program and Progress Towards High Beta, Long Pulse Operating Scenarios”, paper OV/2-2. This conference.
[33] R.Maingi et al., “H-mode Research in NSTX”, paper EX/C2-5. This conference
[34] V.K.Gusev et al., “New Results from Globus-M Spherical Tokamak”, paper EX/P3-10. This conference
[35] O.Motojima et al., “Recent Advance in LHD Experiment”’ OV/1-6, this conference.
[36] F.Wagner et al., “Major Results from Wendelstein 7-AS Stellarator”, paper OV/2-4. This conference.
[37] C.Alejaldre et al., “Magnetic Configuration and Transport Interplay in the TJ-II Flexible Heliac Configuration, paper OV/4-4. This conference.
[38] J.S.Sarff et al., “Overview of Improved Confinement and Plasma Control in the MST Reversed Field Pinch.”. paper OV/4-3. This conference.

[39] P.Martin et al., “Overview of Quasi Single Helicity Experiments in Reversed Field Pinches”, paper EX/C1-2. This conference.
[40] T.Cho et al, “Extended Consolidation of Scaling Laws of Potentials Covering over the Representative Tandem-mirror Operations in GAMMA-10, paper EX/C1-4Ra. This conference;
[41] E.P.Kruglyakov et al., “Axisymmetric Magnetix Mirrors for Plasma Confinement; Recent Development and Perspectives, paper EX/C1-4Rb. This conference
[42] J.Y.Kim et al., “RF-heating and Plasma Confinement Studies in HANBIT Mirror Device”, paper EX/C1-4Rc. This conference.

List of Used Acronyms.

ATS	Advanced Tokamak Scenarios
BES	Beam Emission Spectroscopy
DND	Double Null Divertor
ECE	Electron Cyclotron Emission
EBWH	Electron Bernstein Wave heating
ECW	Electron Cyclotron Waves
ECCD	Electron Cyclotron Current Drive
ECRH	Electron Cyclotron Resonant Heating
ELM	Edge Localized Modes
ETGM	Electron Temperature Gradient Mode
FRC	Field Reversed Configuration
HFS	High Field Side
HHFW	High Harmonic Fast Wave
e-ITB	electron Internal Transport Barrier
i-ITB	ion Internal Transport Barrier
H-mode	High Confinement mode
IBWH	Ion Bernstein Wave Heating
ICRH	Ion Cyclotron Resonant Heating
ITGM	Ion Temperature Gradient Mode
LFS	Low Field Side
LHCD	Lower Hybrid Current Drive
LHRH	Lower Hybrid Resonant heating
L-mode	Low Confinement mode
NBIH	Neutral Beam Injection Heating
NTM	Neoclassical Tearing Mode
PPCD	Pulsed Poloidal Current Drive
QSH	Quasi Single Helicity
RFP	Reversed Field Pinch
RLW	Rebut-Lallia-Watkins
SND	Single Null Divertor
SH	Single Helicity
TEM	Trapped Electron Mode